Use of Radiation Detection, Measuring, and Imaging Instruments to Assess Internal Contamination from Intakes of Radionuclides

Part II: Field Tests and Monte Carlo Simulations Using Anthropomorphic Phantoms

Prepared by

R. Anigstein, R. H. Olsher, and J. C. Engdahl

S. Cohen & Associates
1608 Spring Hill Road
Vienna, Virginia 2218

Under

Contract Number 200-2002-00367
Task Order Number 0007

Prepared for

Centers for Disease Control and Prevention
National Center for Environmental Health
Radiation Studies Branch

Phillip Green
Project Officer

June 19, 2007

Contents

Contents (continued)

Page

Tables

Page

Figures

Page

PREFACE

Part I of the present series described a study to evaluate radiation detection and imaging systems commonly found in hospitals to determine their suitability for rapidly scanning individuals for internal contamination, and to develop recommendations regarding their potential use (Anigstein et al. 2007). That report described the measurement of count rates from single discrete radioactive sources of ^{60}Co, ^{137}Cs, ^{192}Ir, and ^{241}Am, using a Philips AXIS gamma camera, an Atomlab thyroid uptake system, and a Ludlum waste monitor. The sources were measured in air at various distances from the detector and at various positions within a simplified phantom constructed of square acrylic slabs. A Monte Carlo computer model of the Philips AXIS camera was developed and validated against the experimental in-air measurements. The model was then applied to calculating count rates on two models of the AXIS camera from radionuclides uniformly distributed in the lungs of a stylized mathematical phantom of the human body, based on the ORNL phantom series described by Cristy and Eckerman (1987).

The current work extends the earlier investigation by using realistic anthropomorphic phantoms to study the responses of four instruments to five radionuclides distributed in the lungs. The experimental measurements were performed on a Rando Phantom—an anthropomorphic phantom that contains a human skeleton embedded in a tissue-equivalent urethane rubber. The five radionuclides—^{60}Co, ^{90}Sr, ^{137}Cs, ^{192}Ir, and ^{241}Am—were selected from the 10 nuclides cited by the DOE/NRC Interagency Working Group on Radiological Dispersion Devices as being among the "isotopes of greatest concern" (DOE/NRC 2003, Appendix F). Ten encapsulated sources of each nuclide were placed in pre-drilled holes in the lung region of the phantom. Count rates from each nuclide were measured on the Siemens e.cam Fixed 180 gamma camera, an Atomlab thyroid probe, a Ludlum survey meter, and a Ludlum waste monitor.

We calculated calibration factors that relate count rates on these instruments to lung burdens of each of the five nuclides, using the Los Alamos MCNPX (Monte Carlo N Particle eXtended) computer code. We first constructed a mathematical model of each of the instruments, using engineering drawings and other data obtained from the manufacturers. We combined this model with an MCNP model of a Rando Phantom, constructed from CT scans of this phantom (Wang et al. 2004). We used the combined model to simulate the response of each instrument to sources in the phantom, and compared the calculated results to the experimental measurements. The agreement between the calculated and measured responses validated the MCNP models of the four instruments. We next calculated calibration factors for each instrument by combining the model of the instrument with the NORMAN phantom, in a configuration similar to one that would be used in a clinical setting. NORMAN was developed by the Health Protection Agency in the United Kingdom from an MRI scan of a volunteer (Jones 1997), adjusted to the size and weight of Reference Man (ICRP 2002).

The authors gratefully acknowledge the support and assistance of a number of individuals and organizations, without whom this work would not have been possible. These include the Radiology Department of the New York University Medical Center, which provided access to

the equipment in the Nuclear Medicine Section, and Dori Landsman, of the Nuclear Medicine Section, who assisted in operating the equipment. Christopher Marshall, Director of Radiation Safety for the Medical Center, arranged for the use of radioactive sources at Tisch Hospital, provided access to the radioactive waste monitors, and gave helpful advice and suggestions. Prof. Burton Budick of the New York University Physics Department arranged a loan of the Rando Phantom.

We wish to thank Peter Dimbylow of the Radiation Protection Division of the Health Protection Agency for providing access to the NORMAN database. Our thanks also to Keith Eckerman of the Oak Ridge National Laboratory, who provided advice and software to model the â spectra of ^{90}Sr and ^{90}Y; and to X. George Xu, Associate Professor of Nuclear and Biomedical Engineering, Rensselaer Polytechnic Institute, who provided the MCNP model of a Rando Phantom.

Several commercial firms provided valuable support and assistance. Jim Caruba of Siemens Medical Solutions USA furnished engineering drawings and other data, and gave freely of his time answering questions; this support enabled us to construct a detailed mathematical model of the Siemens e.cam Fixed 180 gamma camera. Jamie Witt and Rollie Cantu of Ludlum Measurements, Inc., provided engineering drawings and detailed technical information on the Ludlum Model 19A Survey Meter and the Model 3530 Waste Monitor, enabling us to construct models of these instruments. Clyde Schein of Biodex Medical Systems provided information on the Atomlab 950 Thyroid Uptake System, as did Dan Herr of Saint-Gobain Crystals. Lila Corwin, Director of Marketing Communications, Biodex Medical Systems, graciously permitted us to use the illustration of the Atomlab 950 Thyroid Uptake System shown in Figure 1-6. The illustration of the Atomlab Thyroid Probe shown in Figure 1-7 was copied from “Atomlab 950 (PC) Medical Spectrometer Service/Operation Manual,” published by Biodex Medical Systems, Inc., Shirley, NY. Lissa Tegelman of Isotope Products Laboratories designed the source capsules and facilitated the production and delivery of the custom-made sources on a very tight and aggressive schedule. Joshua Levy, president of The Phantom Laboratory, furnished advice and information, and donated spare parts for the Rando Phantom.

Chapter 1

RADIATION MEASUREMENTS

1.1 Introduction

A radiological emergency, such as the detonation of a radioactive dispersion device (RDD or "dirty bomb"), could lead to the inhalation of airborne radioactive material by a large number of people. There would be a need to rapidly measure this inhaled activity and determine the need for medical intervention. Anigstein et al. (2007) demonstrated that radiation detection and imaging systems commonly found in hospitals can be used to screen exposed individuals for radioactive materials inside the body. The current study extends the earlier investigation by using realistic anthropomorphic phantoms to study the responses of four instruments to five radionuclides distributed in the lungs.

The present chapter describes experiments to determine the response of these instruments to radioactive sources in the lung region of the anthropomorphic Rando Phantom. The studies were performed at the Tisch Hospital of the New York University Medical Center in New York City. Measurements were performed on a Siemens e.cam Fixed 180 gamma camera, a Biodex Atomlab 950 Thyroid Uptake System, a Ludlum Model 19A Micro R survey meter, and a Ludlum 3530 Radioactive Waste Monitor. All these instruments are equipped with thallium-doped sodium iodide (NaI[Tl]) scintillation detectors. The first three instruments are located in the Nuclear Medicine Section of the Department of Radiology. The waste monitor is located at the entrance to a loading dock of the hospital used for the disposal of solid wastes.

1.2 Materials and Equipment

1.2.1 The Rando Phantom

The Rando Phantom used in the present study, originally marketed by Alderson Research Laboratories, USA, as the Rando Average-Man Phantom, was described by Alderson et al. in 1962 (cited by Shrimpton et al. 1981).[1] This phantom, similar to the one illustrated in Figures 1-1 and 1-2, contains a natural human skeleton embedded in a urethane rubber. This rubber has an effective atomic number and mass density that closely simulate muscle tissue with randomly distributed fat. The Rando Phantom's lung material closely mimics the density of lungs in a median respiratory state. This phantom is widely used in treatment planning for radiation therapy.

The phantom utilized in the present study represents an adult male, 5 ft 9 in (175 cm) tall, weighing 162 lb (73.5 kg). As shown in Figure 1-2, the phantom is sectioned into 34 horizontal slabs, each approximately 2.5 cm thick, which comprise the head and torso. There is also a base piece, approximately 10 cm thick, comprising the groin and upper sections of the thighs. Each

[1] The Rando Phantom is currently distributed by The Phantom Laboratory, P.O. Box 511, Salem, NY 12865.

Figure 1-1. Rando Phantom: Assembled (Wang et al. 2004)

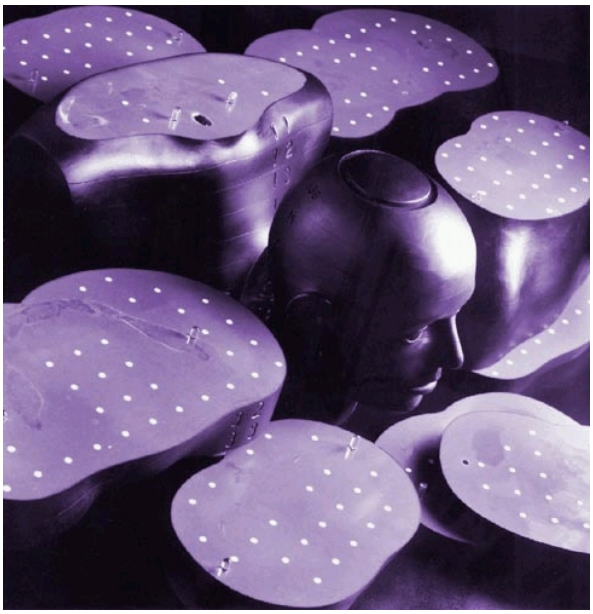

Figure 1-2. Rando Phantom: Sections (The Phantom Laboratory [n/d])

slab contains a 3-cm × 3-cm matrix of vertical holes, 5 mm in diameter. Each hole is filled with a removable wax plug. For ease of handling during the radiation measurements, the head and neck portions were removed. The phantom was mounted on a wooden board which was bolted to a wheeled stand made from a laboratory stool with a screw lift, with the seat cushion removed. This stand facilitated the transfer of the phantom and allowed continuous adjustments of its vertical and horizontal positions.

1.2.2 Radioactive Sources

The study addressed five radionuclides: ^{60}Co, ^{90}Sr, ^{137}Cs, ^{192}Ir, and ^{241}Am. These nuclides were selected from the 10 nuclides cited by the DOE/NRC Working Group as being among the "isotopes of greatest concern" (DOE/NRC 2003, Appendix F). Four of these five nuclides were studied by Anigstein et al. (2007). The fifth nuclide, ^{90}Sr, has been widely used as a heat source in thermoelectric generators and thus may pose potential risks. Unless freshly separated, ^{90}Sr is in secular equilibrium with its short-lived progeny, ^{90}Y ($t_{½}$ = 64 h), which emits β rays with a

maximum energy of 2.28 MeV. Thus, although both ^{90}Sr and ^{90}Y are almost pure β emitters,[2] the high-energy ^{90}Y β rays create a strong source of bremsstrahlung radiation that can be detected by NaI(Tl) detectors. Of the other nuclides on this list, ^{238}Pu was eliminated on the basis of Monte Carlo calculations that indicated that to produce counts in a gamma camera (the most sensitive of the four instruments) that are comparable to the measured background would require a lung burden of about 20 μCi (740 kBq).[3] An intake of such an activity would result in a committed dose of more than 1,000 rem (10 Sv). Therefore, the radiation detectors in the present study would not be suitable instruments for screening individuals who may have inhaled this nuclide, since a lung burden below the level of detection could still pose a serious health risk to the exposed individual. Similar considerations apply to ^{210}Po. ^{239}Pu is a fissile material that can be used to fabricate nuclear weapons, and is therefore tightly controlled; it is unlikely that it would be used in an RDD. ^{244}Cm or ^{252}Cf are small neutron sources used in research and measuring instruments.

The design of the Rando Phantom requires the use of discrete, encapsulated radioactive sources that can be inserted into the holes drilled in the phantom. The holes in the lung region provide up to 100 possible source locations. Both procurement costs and the logistics of the experiment limited us to using 10 sources of each nuclide. We performed preliminary Monte Carlo simulations to select the 10 source locations that would produce counts in the gamma camera that most closely corresponded to the counts from a uniform distribution of activity in both lungs. We also calculated the activity of each nuclide that would yield a count rate on the order of 10 kcps in each camera head from the 10 sources in the phantom. These activities were selected so as not to produce significant counting losses in the camera due to the dead time of the detector system, and yet produce adequate responses in the other detectors, which are less sensitive than the gamma camera.

We thereupon procured 10 sources of each nuclide, calibrated against NIST-traceable standards with a certified accuracy that range from ± 3.0% to ± 3.3% at the 99% confidence level.[4] The maximum variation among the individual sources of each nuclide does not exceed 1%, making the individual sources of a given nuclide essentially interchangeable. The combined activities of the sources are presented in Table 1-1.

Each custom-made source is sealed inside an acrylic rod, 1 cm long × 4.8 mm in diameter, as shown in Figure 1-3. The rods were designed to fit the 5 mm-diameter holes in the phantom. The wax plugs in the selected locations in the right lung were trimmed to a length of 1.5 cm to create 1-cm-deep cavities, which could contain the sources.

---

[2] ^{90}Y emits a very low-intensity γ ray and low-energy x rays which are not readily detected: see Section 2.1.4.

[3] A count rate of twice background is a commonly used practical measure of detectable activity during routine screening. Lower limits of detection are achievable—see discussion in Section 3.6.

[4] Supplied by Isotope Products Laboratories, 24937 Avenue Tibbitts, Valencia, CA 91355.

Table 1-1. Radioactive Sources

Nuclide	Half-life (y)	Calibration date	Calibrated activity[a] (kBq)	Date of experiment[b]	Decayed activity (kBq)
Co-60	5.271	6/7/05	43.80	2/12/06	40.03
Sr-90/Y-90[c]	28.79	2/2/06	2,532	2/12/06	2,530
Cs-137	30.07	9/14/05	78.2	2/12/06	77.5
Ir-192	0.2021	12/9/05	71.2	2/12/06	38.70
Am-241	432.2	2/10/06	356	2/19/06	356

[a] Total activity of 10 sources of each nuclide

[b] Dates of gamma camera measurements listed as an example. Source activities were decay-corrected for the actual dates of measurements on other instruments

[c] The ^{90}Sr source material was separated in January 2004, so ^{90}Y was in full secular equilibrium at the time of the experiment.

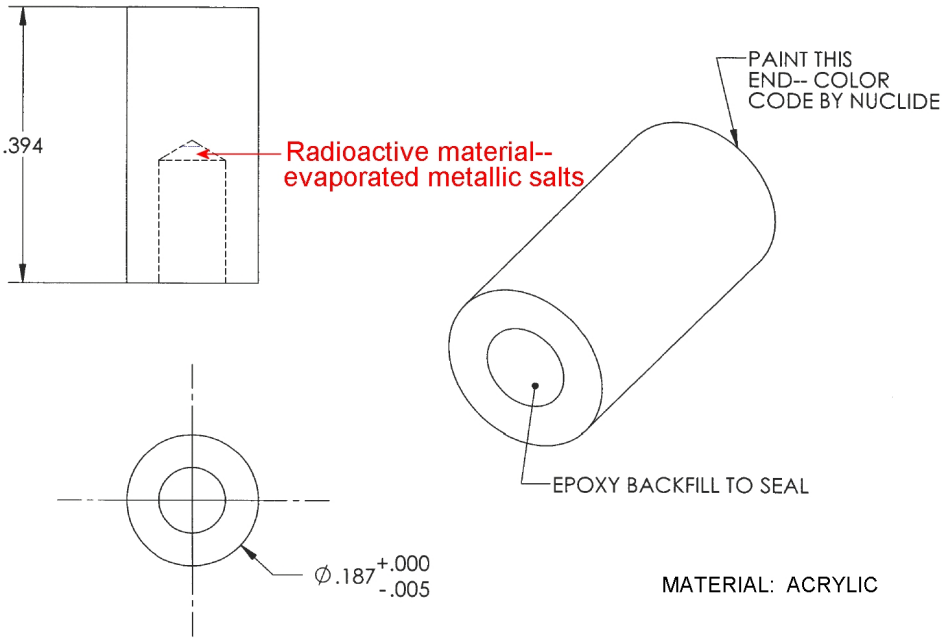

Figure 1-3. Source Capsule (dimensions in inches)

1.2.3 Siemens Gamma Camera

The Siemens e.cam Fixed 180 is representative of the gamma cameras distributed by Siemens Medical Solutions USA, one of the three major U.S. suppliers of imaging equipment for nuclear medicine.[5] As its name implies, the camera consists of two detector heads mounted in fixed positions, 180º apart, on a rotating gantry. According to Siemens (2005), this system is "optimized for both whole body and SPECT scanning with the detectors in opposing position . . .

[5] The others are Philips Medical Systems, N. A. and GE Healthcare.

Figure 1-4. Siemens e.cam Fixed 180 Gamma Camera

Figure 1-5. Siemens e.cam Camera Without Table

The open gantry permits easy access to both detectors for imaging of patients on gurneys and wheelchairs or in a standing position." Figure 1-4 shows the e.cam Fixed 180 with the patient handling table in its normal position; Figure 1-5 shows the same instrument with the table removed, the configuration used in the present study.

The Siemens e.cam is equipped with a ⅜-inch-thick (0.95 cm) NaI(Tl) scintillator, in common with most of the gamma cameras in the United States. Up to six non-overlapping energy windows, with widths of up to 50%, can be used for acquisition of counts and/or images on this system. However, counts can be recorded from a maximum of three channels during a given acquisition. Therefore, when more than three windows are used, two or more windows must be combined into a single channel. The present study used six 50% energy windows for all nuclides except ^{241}Am—two windows were sufficient to span the photon spectrum generated by this nuclide. To determine if the system correctly recorded counts near the low and high ends of the energy range, Channels 1 and 3 were set to the lowest and highest energy windows, respectively, while Channel 2 comprised the middle four windows. In the case of ^{241}Am, the two energy windows constituted separate channels. Table 1-2 lists the windows in each channel, the peak or central energy for each window, and the upper and lower energy limits, equal to the peak energy ± 25%. For convenience, the peak energy of each window, expressed in keV, was set to an integer value, leaving small gaps between the channels.

1.2.4 Atomlab Thyroid Probe

The Atomlab 950 Thyroid Uptake System, made by Biodex Medical Systems, Inc., is illustrated in Figures 1-6 and 1-7. The system includes an adjustable probe which consists of a 2-inch ×

Figure 1-6. Atomlab 950 Thyroid Uptake System (photo courtesy of Biodex Medical Systems, Inc.)

Figure 1-7. Atomlab Thyroid Probe

2-inch (~5-cm × 5-cm) NaI(Tl) scintillator coupled to a photomultiplier tube (PMT). This detector assembly is housed inside a cylindrical lead shield. The front part of the shield is a collimator that is designed to shield the detector from stray radiation outside the thyroid region. The collimator contains a conical cavity that is 6.68 inches (~17 cm) deep and 4.15 inches (10.5 cm) in diameter at the front end, tapering down to 2 inches at the face of the crystal. A simplified schematic diagram showing a cross-section of the probe appears in Figure 2-3. The system includes a multi channel analyzer (MCA). In the present study, the MCA was set to an energy range of 20 – 1,499 keV.

Table 1-2. Energy Windows (keV)

Nuclide:		Co-60, Cs-137			Sr-90, Ir-192			Am-241		
Channel	Window	Peak	Min	Max	Peak	Min	Max	Peak	Min	Max
1	1	41	30.75	51.25	35	26.25	43.75	35	26.25	43.75
2	2	69	51.75	86.25	59	44.25	73.75	59	44.25	73.75
	3	116	87	145	99	74.25	123.75			
	4	194	145.5	242.5	166	124.5	207.5			
	5	324	243	405	277	207.75	346.25			
3	6	541	405.75	676.25	462	346.5	577.5			

1.2.5 Ludlum Survey Meter

The Model 19A Micro R Meter, made by Ludlum Measurements, Inc., is shown in Figure 1-8. This portable radiation monitor is typical of survey meters commonly used in facilities that

Figure 1-8. Ludlum Model 19A Micro R Meter

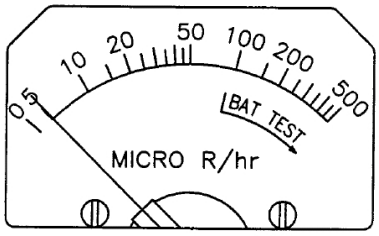

Figure 1-9. Ludlum Model 19A Meter Scale

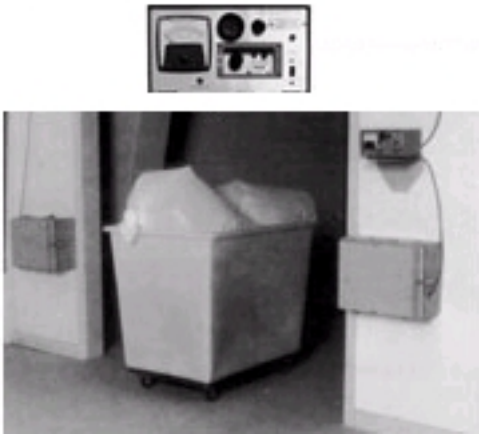

Figure 1-10. Ludlum Model 3530 Radioactive Waste Monitor

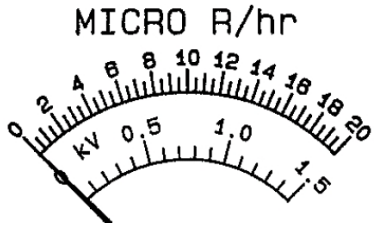

Figure 1-11. Ludlum Model 3530 Meter Scale

handle radioactive materials. The detector is an NaI(Tl) scintillator, 1 inch (~2.5 cm) in diameter and 1 inch thick, that is coupled to a PMT approximately 29 mm in diameter. The detector is encased by an aluminum cap, and the entire detector assembly is housed in an outer tube made of aluminum. The instrument, including the electrical components, is contained in a rectangular box made of cast aluminum.

The output of the detector is displayed on an analog meter with a logarithmic scale that has a range of 0 – 500 μR/h, as shown in Figure 1-9. The electronic circuitry suppresses readings at the low end of the scale.[6] Although the interactions of γ-ray photons with NaI(Tl) detectors are registered as counts, not exposure, the count rate is translated into an exposure rate. The instrument is calibrated so that a scale reading of 5 μR/h corresponds to a count rate of 875 cpm (Ludlum 2000). Since both the counting efficiency and the exposure rate vary with photon energy in a nonlinear manner, the reading is not a true exposure rate.

1.2.6 Ludlum Waste Monitor

The Ludlum 3530 Radioactive Waste Monitor, illustrated in Figures 1-10 and 1-11, consists of two detectors yoked together to a single display/alarm unit. Each detector consists of an NaI(Tl)

[6] Rollie Cantu, Ludlum Measurements, Inc., private communication with Robert Anigstein, SC&A, Inc., December 1, 2006.

scintillator, 3 inches (~7.6 cm) in diameter and 1 inch (~2.5 cm) thick. The scintillator is coupled to a PMT, 1.5 inches (~38 mm) in diameter, by means of a 0.25-inch-thick (6.25-mm), 3-inch diameter quartz light pipe. Each detector is housed in a lead shield that is approximately 0.75 in (~1.9 cm) thick. The meter, which displays the sum of the signals from both detectors, has a linear scale with a range of 0 – 20 μR/h. A scale reading of 1 μR/h corresponds to a combined count rate of 2400 cpm.[6] Each detector assembly is contained in a separate sheet steel housing, with an opening that is 3 inches high by 5 inches wide (7.6 × 12.7 cm), covered by a ⅛-inch-thick (0.32-cm) acrylic window.

In the installation at Tisch Hospital, the detectors are mounted on opposite sides of the doorway leading to the loading dock used for the disposal of solid wastes. The detectors are at an average height of 83 cm above the floor. The distance between the acrylic windows of the two detectors is approximately 195 cm. Since the purpose of the monitor is to sound an alarm if any radioactive material passes through the doorway, the unit is not routinely calibrated, so the readings do not necessarily correspond to an actual exposure rate.

1.3 Radiation Measurements

1.3.1 Gamma Camera

Measurements were performed with the Siemens e.cam camera, using both detectors with the collimators removed. The Rando Phantom was centered between the two detectors. The height of the stand was adjusted so that the position of the phantom was similar to that of a patient undergoing a planar lung scan, with the two detectors recording anterior and posterior views. The front and back of the phantom were approximately 5 cm from the aluminum windows covering the detectors. Such a separation would be needed in the event that the camera were used to assess an exposed individual: without a collimator, there is no pressure-sensitive alarm to protect the patient from potential injury by contact with the detector, nor to protect the detector from being damaged by contact with the patient.

We used the following procedure to record the count rates from each of the five radionuclides. First, we adjusted the energy windows for the given nuclide (see Table 1-2). Next, we placed the phantom, without sources, in the position described above, and recorded 2-minute background counts in each channel of each detector. Next, we removed the phantom and placed 10 sources of the given nuclide in selected positions in the right lung, as described on page 3. We then replaced the phantom between the detectors and counted for 2 minutes.

The observed count rates are listed in Table 1-3. The uncertainty of the count rates in any one channel (expressed as the coefficient of variation) is less than 1%, while the uncertainty of the total net count rates from each of the five nuclides ranges from 0.08% to 0.14%. A more significant source of experimental error is the activities of the radioactive sources, which have uncertainties of up to 3%.

Table 1-3. Measurements with Siemens e.cam Gamma Camera

Nuclide	Activity[a] (kBq)	Channel	Sources (cps)		Background (cps)		Net normalized count rate (cps/Bq)		Coefficient of variation	
			Anterior	Posterior	Anterior	Posterior	Anterior	Posterior	Anterior	Posterior
Co-60	40.0	1	238	236	36	39	5.06e-03	4.93e-03	0.75%	0.77%
		2	5,236	5,102	722	759	1.13e-01	1.09e-01	0.16%	0.16%
		3	805	762	65	70	1.85e-02	1.73e-02	0.36%	0.38%
		Total	6,279	6,100	823	867	1.36e-01	1.31e-01	0.14%	0.15%
Sr-90/ Y-90	2,530	1	1,164	1,285	21	23	4.52e-04	4.99e-04	0.27%	0.26%
		2	9,568	9,892	729	751	3.49e-03	3.61e-03	0.10%	0.10%
		3	253	261	74	81	7.10e-05	7.10e-05	0.92%	0.94%
		Total	10,985	11,438	824	855	4.02e-03	4.18e-03	0.10%	0.10%
Cs-137	77.5	1	358	373	36	39	4.16e-03	4.32e-03	0.56%	0.55%
		2	6,498	6,435	722	759	7.46e-02	7.33e-02	0.13%	0.14%
		3	1,081	1,027	65	70	1.31e-02	1.24e-02	0.30%	0.32%
		Total	7,937	7,834	823	867	9.18e-02	9.00e-02	0.12%	0.12%
Ir-192	38.7	1	294	317	21	23	7.05e-03	7.60e-03	0.59%	0.57%
		2	10,387	10,662	729	751	2.50e-01	2.56e-01	0.10%	0.10%
		3	1,071	1,135	74	81	2.58e-02	2.72e-02	0.31%	0.30%
		Total	11,752	12,114	824	855	2.82e-01	2.91e-01	0.09%	0.09%
Am-241	356	1	2,880	2,655	31	33	8.00e-03	7.37e-03	0.17%	0.18%
		2	10,504	10,499	111	123	2.92e-02	2.91e-02	0.09%	0.09%
		Total	13,384	13,154	142	156	3.72e-02	3.65e-02	0.08%	0.08%

[a] At time of measurements

1.3.2 Thyroid Probe

The thyroid probe was oriented in a horizontal position, centered on the chest of the Rando Phantom. A 5-minute background count was recorded prior to each set of measurements. Next, the phantom with the sources inside was positioned facing the detector, the chest approximately 50 cm from the outer edge of the collimator, and a 5-minute count was recorded. This distance was selected so that the angle subtended by the conical collimator would encompass the lung region of the phantom. Next, the phantom was turned with its back toward the detector, and another 5-minute count was taken. The actual distances from the phantom to the collimator ranged from 48 to 54 cm during the various measurements. The recorded count rates are listed in Table 1-4.

The coefficient of variation is higher than for the gamma camera, despite the longer counting time. This is due to the smaller number of gross counts, resulting from a lower counting efficiency and a greater distance from the source to the detector. Again, the uncertainties in the activities of the sources make a significant contribution to the experimental error.

Table 1-4. Measurements with Atomlab 950 Thyroid Uptake System

Nuclide	Activity[a] (kBq)	Back-ground (cps)	Count rate from sources (cps)		Net normalized count rate (cps/Bq)		Coefficient of variation		Distance[b] (cm)	
			Anterior	Posterior	Anterior	Posterior	Anterior	Posterior	Anterior	Posterior
Co-60	40.2	9.0	27.9	29.0	4.69e-04	4.96e-04	1.9%	1.8%	65.0	67.0
Sr-90/Y-90	2,529	11.4	27.2	31.2	6.27e-06	7.82e-06	2.3%	1.9%	67.0	67.0
Cs-137	77.6	8.5	31.9	33.7	3.01e-04	3.24e-04	1.6%	1.5%	71.0	71.0
Ir-192	43.7	8.8	36.4	40.0	6.31e-04	7.12e-04	1.4%	1.3%	67.0	69.2
Am-241	356	9.2	29.1	35.2	5.59e-05	7.30e-05	1.8%	1.5%	67.0	67.0

[a] At time of measurements

[b] From aluminum window to phantom

1.3.3 Survey Meter

Prior to making any measurements, we adjusted the analog display of the survey meter to zero, with the switch in the off position. We then placed the instrument against the chest of the Rando Phantom and moved it up and down the sternum until we found the location with the highest reading, which was recorded as the exposure rate in the anterior position. Although the sources were located only in the right lung, we used the medial position to replicate the clinical situation, in which the activity would be distributed in both lungs. We next placed the meter against the upper back of the phantom and moved it along the spine to again find the highest reading, which was recorded as the posterior exposure rate. In an attempt to measure the background, we took the meter to a location remote from any sources of radiation, and found that the meter read zero. This is most likely due to the voltage threshold in the logarithmic circuitry of the instrument, which suppresses readings from low count rates.

Table 1-5 lists the observed exposure rates and the calculated count rates, assuming a conversion factor of 175 cpm per μR/h (the calibration of the meter is discussed on page 7). The main source of experimental error is reading the meter scale, shown in Figure 1-9. The uncertainty in the reading is estimated to be ± 10%, which overshadows the statistical uncertainty. Additional but unknown sources of error are uncertainty in the calibration and the lack of a background reading.

1.3.4 Waste Monitor

The Rando Phantom containing the sources was placed in front of one the detectors of the waste monitor, with the lungs centered on the detector. The base of the stand on which the phantom was mounted and a curb-like protrusion on the floor in front of the detector prevented the phantom from being placed less than 26 cm from the acrylic window. The anterior exposure rates were recorded with the phantom facing the nearest detector, with its back toward the more remote detector. The posterior readings were recorded with the position reversed. Meter

readings were produced by the combined signals from both detectors. The exposure rates and the calculated count rates are listed in Table 1-6.

Table 1-5. Measurements with Ludlum 19A Micro R Meter

Nuclide	Activity[a] (kBq)	Recorded exposure rate (μR/h)		Calculated count rate[b] (cps)		Net normalized count rate (cps/Bq)	
		Anterior	Posterior	Anterior	Posterior	Anterior	Posterior
Co-60	40.3	25	25	73	73	1.8e-03	1.8e-03
Sr-90/Y-90	2,529	35	45	102	131	3.5e-05	4.0e-05
Cs-137	77.6	25	25	73	73	9.4e-04	9.4e-04
Ir-192	43.7	50	65	146	190	3.3e-03	4.3e-03
Am-241	356	30	35	88	102	2.5e-04	2.9e-04

[a] At time of measurements

[b] Based on conversion factor: 1 μR/h = 175 cpm (see page 7)

Table 1-6. Measurements with Ludlum 3530 Waste Monitor

Nuclide	Activity[a] (kBq)	Recorded exposure rate (μR/h)		Calculated count rate[b] (cps)		Net normalized count rate (cps/Bq)	
		Anterior	Posterior	Anterior	Posterior	Anterior	Posterior
Co-60	40.3	3	3	120	120	3.0e-03	3.0e-03
Sr-90/Y-90	2,529	3	4.5	120	180	4.7e-05	5.5e-05
Cs-137	77.5	3	3	120	120	1.5e-03	1.5e-03
Ir-192	43.7	5	5	200	200	4.6e-03	4.6e-03
Am-241	356	3	3.5	120	140	3.4e-04	3.9e-04

[a] At time of measurements

[b] Based on conversion factor: 1 μR/h = 2400 cpm (see page 7)

As was the case with the survey meter, the main source of experimental error was reading the meter scale, illustrated in Figure 1-11. The uncertainty in the reading is estimated to be 0.25 μR/h, which corresponds to an uncertainty of 5% – 10% over the range of observed exposure rates. This overshadows the statistical uncertainty. An additional but unknown source of error is uncertainty in the calibration of the instrument and lack of a background reading: the meter read zero in the absence of the sources. The lead shielding on the back and sides of the detector would significantly lower the background. This shielding and a possible offset of the meter scale would explain the zero readings.

1.4 Summary and Conclusion

Measurements were performed on sources of five different radionuclides located in the lung region of the Rando Phantom, using four different radiation detection systems at the NYU Medical Center. All instruments produced readings that were significantly above background, showing that these instruments are potentially useful in assessing lung burdens of these nuclides.

Chapter 2

MONTE CARLO SIMULATIONS OF EXPERIMENTAL MEASUREMENTS

This chapter discusses the use of Monte Carlo computer models to simulate the experimental measurements presented in Chapter 1. The first step of the analysis was to construct mathematical models of the radiation detectors. We then simulated the radiation response of these models, using the same geometries described in Chapter 1, and compared the calculated results to the experimental observations. The aim of these comparisons is to validate the models of the instruments. As described in Chapter 3, these models are used to derive calibration factors for these instruments, enabling their use in assessing the lung burdens of exposed individuals.

2.1 Methodology

The analysis of the radiation response of the four detectors used in our study required the construction of a mathematical model of each instrument. It also required a mathematical model of the radiation source, and a model to simulate the transport of radiation from the source to the detector. We will begin by describing the radiation transport model used in these calculations.

2.1.1 Radiation Transport Model

Radiation transport was modeled by means of the Los Alamos Monte Carlo code MCNPX Version 26C. LANL (2006) presents the following description of this code:

> MCNPX is a general-purpose Monte Carlo radiation transport code for modeling the interaction of radiation with everything. MCNPX stands for Monte Carlo N-Particle eXtended. It extends the capabilities of MCNP4C3 to nearly all particle types, to nearly all energies, and to nearly all applications without an additional computational time penalty. MCNPX is fully three-dimensional and time dependent. It utilizes the latest nuclear cross section libraries and uses physics models for particle types and energies where tabular data are not available.

A more detailed description is provided by Hendricks et al. (2006). The present analysis utilized the MCNPLIB04 photon cross-section library, which was released in 2002 and is the latest release to date. This library is based on the Evaluated Nuclear Structure Data File (ENSDF), which is updated and maintained by the National Nuclear Data Center at the Brookhaven National Laboratory.

For the purpose of the present analysis, MCNPX is superior to MCNP5, which was used in earlier studies (Anigstein et al. 2007). A key advantage is its ability to efficiently utilize large lattice arrays, such as those of the voxel phantoms, described later.

The calculations utilized the MCNP pulse height tallies, which record the detector events that fall into specified energy bins, such as those corresponding to the energy windows displayed in

Table 1-2. The results are recorded as count per photon, and represent the probability that a photon emitted by the source would produce a pulse within the specified energy range. As explained by LANL (2004):

> The pulse height tally provides the energy distribution of pulses created in a cell that models a physical detector. It also can provide the energy deposition in a cell . . . . The pulse height tally is analogous to a physical detector. The . . . energy bins correspond to the total energy deposited in a detector in the specified channels by each physical particle.

The MCNP analyses of $^{90}Sr/^{90}Y$ utilized the coupled photon-electron mode, in which both primary and secondary electrons (including β particles) were tracked in the medium surrounding the sources in order to model bremsstrahlung production. The analyses of the other nuclides, in which electron transport does not play a significant role, were performed in the photon transport mode.

2.1.2 MCNP Model of Rando Phantom

Wang et al. (2004) created an MCNP model of a Rando Phantom based on data from a CT scan of the phantom. The phantom, similar to the one used our experiments, represented the torso of an adult male. The authors created a three-dimensional image of the phantom by segmenting 175 two-dimensional slices. The model comprises 1,234,800 voxels, each 4.8 mm × 4.8 mm × 5 mm high.

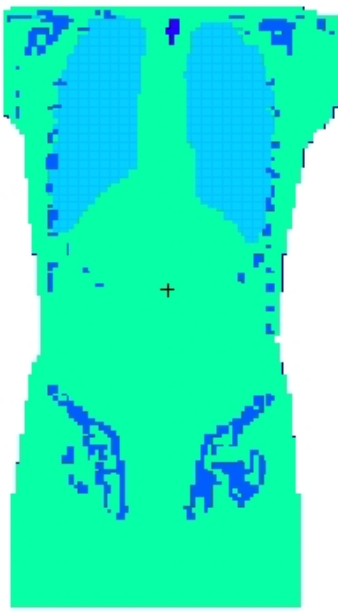

Figure 2-1. MCNP Model of Rando Phantom

White (1978) lists the elemental composition of lung and muscle in the Rando Phantom, while Eckerman et al. (1996) list the composition of natural bone. We incorporated these compositions, listed in Table 2-1, into the model created by Wang et al. to replicate the Rando Phantom used in our studies.[7]

A frontal section of the MCNP model is shown in Figure 2-1. Because the phantom used in the radiation measurements did not include the head and neck sections, the corresponding MCNP model was truncated in the same manner. For all nuclides except ^{90}Sr, the sources were modeled as geometric points. Because the composition of the material surrounding the source can significantly affect bremsstrahlung production, the analyses of the $^{90}Sr/^{90}Y$ sources included explicit models of the source capsules, described in Section 1.2.2.

[7] The composition and densities of the Rando tissues are different from those in current models of the Rando Phantom. However, the data presented by White (1978), which apparently characterize the Rando Phantoms available at the time of publication, are appropriate for the current application, since the Rando Phantom used in the present study was procured in 1978.

Table 2-1. Tissue Composition of Rando Phantom (%)

Element	Lung[a]	Muscle[a,b]	Skeleton[c]
H	5.74	8.87	7.337
C	73.94	66.81	25.475
N	2.01	3.10	3.057
O	18.14	21.13	47.893
F			0.025
Na			0.326
Mg			0.112
Si			0.002
P			5.095
S			0.173
Cl			0.143
K			0.153
Ca			10.19
Fe			0.008
Zn			0.005
Rb			0.002
Sr			0.003
Sb	0.16	0.08	
Pb			0.001
Density (g/cm^3)	0.32	1.00	1.40

[a] White (1978)

[b] All regions of phantom other than lungs or skeleton

[c] Eckerman et al. 1996

We observed some anatomical differences between the voxel model of the phantom and the phantom used in our experiments. For example, inspection of one slice of the chest of the voxel phantom showed that it is about 2 cm smaller in the anterioposterior dimension, and about 1 cm wider in the lateral dimension, than the corresponding slice of the experimental phantom.

2.1.3 Models of Radiation Detectors

Models of the four radiation detection systems were constructed on the basis of engineering drawings and other data obtained from the manufacturers of these instruments. Some of the information is proprietary and confidential—such information can be discussed only in general terms.

Siemens e.cam Fixed 180

Similar to other gamma cameras used for SPECT (single photon emission tomography) studies and for planar images, the Siemens e.cam Fixed 180 consists of a large planar NaI(Tl) crystal,

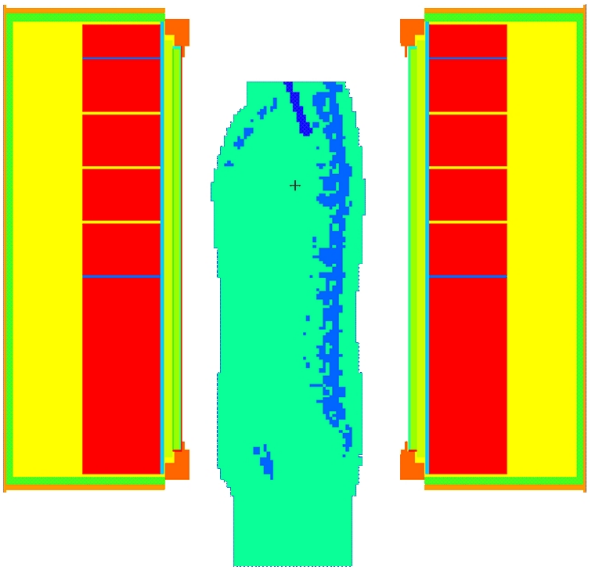

Figure 2-2. Sagittal Section of MCNP Model of Rando Phantom and Siemens e.cam

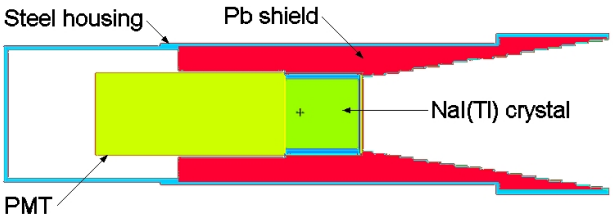

Figure 2-3. MCNP Model of Atomlab Thyroid Probe

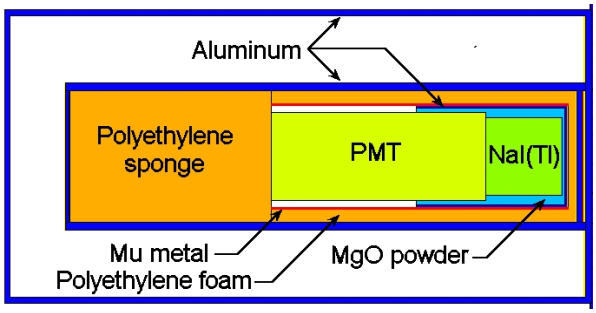

Figure 2-4. MCNP Model of Ludlum 19A Micro R Meter

optically coupled to a glass plate that in turn is coupled to an array of PMTs. The entire assembly is enclosed on five sides by a heavy lead shield to prevent stray radiation from reaching the crystal. The borders of the crystal are partially covered by the lead shield. However, the camera system also imposes an electronic mask over the crystal that creates a dead zone in the margins. Thus, scintillation events near the edges of the crystal which cannot be properly localized by the PMTs are not counted. The active area of the crystal, called the intrinsic field of view, is 53.3 cm high × 38.7 cm wide.

The MCNP model of the gamma camera exposure geometry replicated the conditions of the experiment, described in Section 1.3.1. Figure 2-2 is a sagittal section that shows the position of the voxel model of the Rando Phantom with respect to the two heads of the gamma camera.

Atomlab Thyroid Probe

The MCNP model of the thyroid probe, a component of the Atomlab 950 Thyroid Uptake System, is illustrated in Figure 2-3. This is a simplified model: the rear enclosure of the PMT is shown as a closed steel shell, while the actual instrument has lead shielding inside the PMT enclosure and is open at the end. The experimental measurements were taken at two locations, at the front and back of the phantom, using a single instrument. In order to expedite the analysis, the MCNP model included replicas of the thyroid probe in both locations, allowing the two pulse height tallies to be collected during a single simulation. Given the distance separating the two detectors, backscatter from the duplicate probe would have a negligible effect on the calculated count rates.

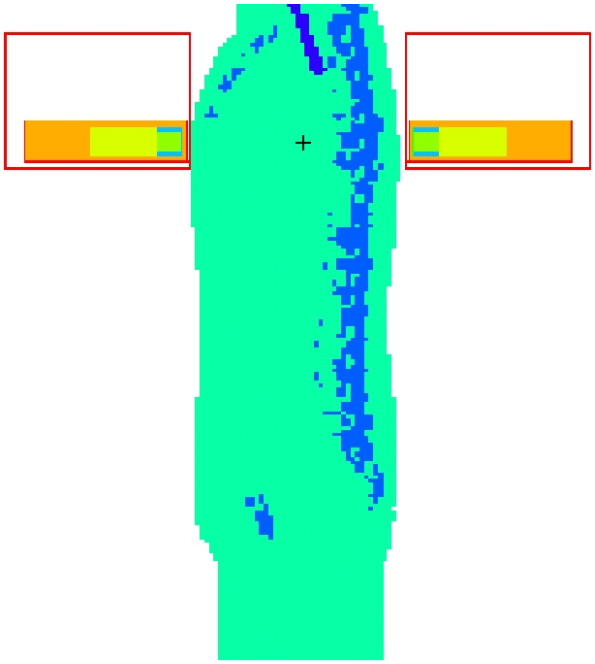

Figure 2-5. MCNP Model of Rando Phantom with Survey Meter

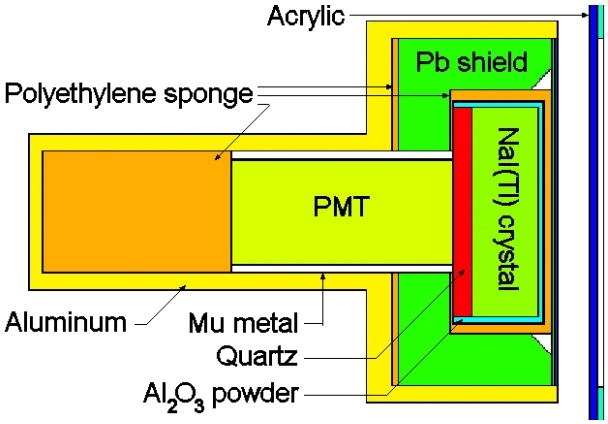

Figure 2-6. MCNP Model of Ludlum 3530 Waste Monitor

Ludlum 19A Micro R Meter

The MCNP model of the Ludlum 19A Micro R Meter, illustrated in Figure 2-4, is based on information furnished by Ludlum Measurements, Inc. The model incorporates the detailed description of the detector assembly, but does not include other components inside the box, such as the batteries and other electrical components. As was the case for the thyroid probe, the survey meter was modeled simultaneously in two locations, as shown in Figure 2-5, although the actual measurements were taken with a single instrument. Given the relatively small mass of the instrument, and the fact that it is primarily made of aluminum, backscatter from the additional meter would have a negligible effect on the calculated count rates.

Ludlum Model 3530 Waste Monitor

The MCNP model of the Ludlum Model 3530 Waste Monitor, shown in Figure 2-6, is also based on information furnished by the manufacturer. The model incorporates the detailed description of the detector assembly, but does not include other components inside the box, such as the electrical components. As discussed in Section 1.2.6, two detectors were connected to the meter during the actual measurements. Whereas the NaI(Tl) crystal in the nearest detector was about 40 cm from the centroid of the sources, the second detector was about 160 cm away. At this distance, the second detector would not significantly affect the meter readings, given the low precision of the instrument, and was therefore not included in the MCNP model. Instead, the first detector was modeled simultaneously in two locations, so that tallies for both anterior and posterior views could be collected in a single computer simulation.

2.1.4 Photon Spectra of Radionuclides

The principal source of the decay schemes of radionuclides in the present study were the DECDC decay data (JAERI 2001), which are based on decay data sets from the August 1997 version of the Evaluated Nuclear Structure Data Files (ENSDF). The "WWW Table of Radioactive Isotopes" (TORI) (Chu et al. 1999) presents more recent data for ^{137}Cs and ^{192}Ir, which were used in the analyses of these nuclides. This Web-based data set, which is also accessible via http://ie.lbl.gov/toi/, provides direct links to the ENSDF that enable the user to access data more recent than those in the TORI tables. Such data were used whenever available.

Table 2-2 lists the spectrum of each γ-emitting nuclide used in the present analysis. Each spectrum encompasses over 99.9% of the total intensity of photons above the minimum energy of 13.5 keV. X rays with energies less than 13.5 keV were not included, since they would either be below the energy range of the instruments and/or be strongly absorbed in the media between the source and the detector.

In the case of ^{90}Sr/^{90}Y, the initial beta spectra were taken from the JAERI tables. However, the energy intervals are spaced logarithmically, with wide intervals in the higher energy region where most of the bremsstrahlung x rays are generated. Because these energy steps were too widely spaced to enable accurate interpolation by MCNP, we created a high-resolution β spectrum by performing a cubic spline interpolation on the JAERI data, using software developed by Eckerman (2006).

Other radiation emitted by the ^{90}Sr/^{90}Y decay chain includes a 2,186-keV γ ray emitted by ^{90}Y with an intensity of 1.4×10^{-6} per 100 disintegrations, and zirconium K x rays with energies of 15 – 18 keV. The total yield of all these photons is 2.6×10^{-3} per 100 disintegrations. A preliminary MCNP analysis showed that these photons made no significant contribution to the calculated count rate from ^{90}Sr/^{90}Y. ^{90}Y also emits conversion electrons with energies of about 1,750 keV at an intensity of 0.0115 per 100 disintegrations. These electrons would make no significant contribution to the electron intensities from β emission and to the ensuing bremsstrahlung intensities. Consequently, these photons and electrons were not included in the present analysis.

2.1.5 Gaussian Energy Distribution

Energy deposited in the NaI(Tl) crystal produces a scintillation which in turn generates an electrical pulse in the camera system. The inherent statistics of the underlying processes produce a Gaussian broadening of the photopeak. These processes cannot be explicitly modeled in standard Monte Carlo codes. Instead, a Gaussian energy-broadening treatment was applied to the pulse height distribution to account for the energy resolution of the detectors.

$$F(E) = a\sqrt{E}$$

F(E) = FWHM (MeV)

Table 2-2. Photon Spectra of Radionuclides

Co-60		Cs-137		Ir-192		Am-241	
E (keV)	I (%)	E (keV)	I (%)	E (keV)	I (%)	E (keV)	I (%)
1332.5	99.9856	661.657	85.1	316.50791	82.8130	59.5412	35.9
1173.24	99.9736	32.194	3.76	468.07152	47.8328	13.9442	21.93
Total	199.9592	31.817	2.04	308.45692	30.0032	17.7502	18.8165
		36.378	0.68	295.95827	28.6699	16.8352	5.8202
		36.304	0.352	604.41464	8.2316	20.7846	4.5630
		37.255	0.215	612.46564	5.3091	13.7597	2.4518
		37.349	0.0481	66.831	4.5300	26.3448	2.4
		36.652	0.0079	588.5845	4.5150	17.0606	2.2726
		Total	92.203	205.7954	3.3009	17.9921	2.0076
				484.578	3.1850	17.5047	1.2610
				65.122	2.6500	11.8868	1.2281
				63	2.0700	21.4912	0.9672
				61.486	1.2000	21.0991	0.9496
				75.749	1.0290	21.34	0.8693
				374.4852	0.7213	15.8773	0.5043
				416.4714	0.6642	16.1093	0.4211
				75.368	0.5330	33.196	0.126
				201.3112	0.4720	43.423	0.073
				71.414	0.4600	98.97	0.0203
				489.039	0.4431	102.98	0.0195
				77.831	0.3650	Total	102.6009
				884.5418	0.2923		
				283.2668	0.2625		
				71.079	0.2390		
				136.34348	0.1830		
				73.363	0.1620		
				420.532	0.0737		
				1061.48	0.0528		
				78.073	0.0478		
				593.37	0.0426		
				76.233	0.0265		
				280.04	0.0232		
				73.59	0.0188		
				329.312	0.0186		
				110.093	0.0126		
				71.875	0.0113		
				703.98	0.0053		
				176.98	0.0043		
				599.4	0.0039		
				64.514	0.0029		
				485.3	0.0022		
				766	0.0015		
				1378.3	0.0012		
				1089.7	0.0011		
				60.903	0.0011		
				Total	230.4881		

a = 0.03561 ($MeV^{½}$)

E = energy (MeV)

The value of *a* was adjusted to yield a value of $\frac{F(E)}{E} = 0.095$ for E = 0.1405 MeV, the energy-dependent spectral resolution typical of gamma camera systems (9.5% at 140.5 keV). The same function was applied to the spectra calculated for the other instruments in the present study.

2.2 Comparison of MCNP Simulations with Experimental Measurements

2.2.1 Simulation of Gamma Camera

The results of the MCNP analyses of the gamma camera are listed in Table 2-3, together with the experimental count rates previously shown in Table 1-3.

Table 2-3. Count Rates on Siemens e.cam Gamma Camera (cps/Bq)

Nuclide	Channel	MCNP		Experiment		Difference (%)		
		Anterior	Posterior	Anterior	Posterior	Anterior	Posterior	Average
Co-60	1	5.73e-03	5.69e-03	5.06e-03	4.93e-03	-12	-13	-13
	2	1.12e-01	1.21e-01	1.13e-01	1.09e-01	1.0	-11	-4.8
	3	1.64e-02	1.81e-02	1.85e-02	1.73e-02	13	-4.4	4.2
	Total	1.34e-01	1.45e-01	1.36e-01	1.31e-01	1.9	-10	-4.0
Sr-90/ Y-90	1	4.72e-04	5.15e-04	4.52e-04	4.99e-04	-4.4	-3.1	-3.7
	2	2.15e-03	2.61e-03	3.49e-03	3.61e-03	63	38	51
	3	3.26e-05	3.94e-05	7.10e-05	7.10e-05	117	80	99
	Total	2.65e-03	3.16e-03	4.02e-03	4.18e-03	51	32	42
Cs-137	1	4.71e-03	4.96e-03	4.16e-03	4.32e-03	-12	-13	-12
	2	6.98e-02	7.77e-02	7.46e-02	7.33e-02	6.8	-5.6	0.6
	3	1.40e-02	1.66e-02	1.31e-02	1.24e-02	-6.1	-26	-16
	Total	8.73e-02	9.81e-02	9.18e-02	9.00e-02	5.2	-8.3	-1.5
Ir-192	1	1.18e-02	1.18e-02	7.05e-03	7.60e-03	-40	-36	-38
	2	2.72e-01	3.14e-01	2.50e-01	2.56e-01	-8.4	-18	-13
	3	1.22e-02	1.48e-02	2.58e-02	2.72e-02	110	84	97
	Total	2.96e-01	3.41e-01	2.82e-01	2.91e-01	-4.8	-14.6	-9.7
Am-241	1	7.86e-03	8.06e-03	8.00e-03	7.37e-03	1.8	-8.6	-3.4
	2	2.58e-02	3.24e-02	2.92e-02	2.91e-02	13.0	-9.9	1.5
	Total	3.37e-02	4.04e-02	3.72e-02	3.65e-02	10.4	-9.6	0.4

Overall, Table 2-3 shows reasonable agreement between the calculated and experimental values for the four γ emitters: ^{60}Co, ^{137}Cs, ^{192}Ir, and ^{241}Am. The agreement of the total count rates for each nuclide is better than the agreement in the individual energy channels, especially in the case

of ^{60}Co, ^{137}Cs, and ^{192}Ir. The most likely explanation is that the inclusion of energy windows with ranges of up to 676 keV for ^{60}Co and ^{137}Cs, and 577.5 keV for ^{192}Ir and ^{90}Sr, may have distorted the energy calibration of the camera system. These cameras, like other cameras designed for SPECT and planar imaging, are optimized for recording photons of much lower energies. When higher energy windows are included, the energy calibration is no longer linear. Consequently, while the total counts over a wide range of energies may be correctly recorded by the camera, the counts recorded in the individual energy windows may not correspond to the actual energies deposited in the NaI(Tl) crystal.

We observe that the average measured count rates for three of the γ emitters are lower than the corresponding calculated values. The difference is most likely due to dead time of the detector system. A team of Swiss investigators determined the dead time of a Siemens e.cam camera by measuring the count rate as a function of the activity of ^{99m}Tc in a cylindrical phantom composed of poly(methyl methacrylate) (PMMA, commonly known as acrylic) (Baechler et al. 2006). The reported dead time was 4.4 μs. We therefore corrected the total measured count rates for dead-time losses, assuming a 4.4-μs dead time and a nonparalyzable system.[8] The corrections range from 3% to 6%. It should be noted that the dead time of a modern gamma camera varies with the count rate. At high count rates, the pulse width is reduced, allowing higher count rates than would be predicted on the basis of the dead time measured at low count rates.

As shown in Table 2-4, the dead-time corrections produce better agreement between the MCNP calculations and the measured values for ^{60}Co, ^{137}Cs, and ^{192}Ir. The average differences between the corrected count rates from the two views and the corresponding MCNP calculations for the four γ emitters range from -4.3% for ^{192}Ir to 6.7% for ^{241}Am. The root-mean-square (rms) difference between the calculated and corrected values of both anterior and posterior views for the four γ emitters is 8.5%.[9] The statistical uncertainties in the MCNP calculations average 0.04%, while the uncertainties in the total measured count rates, listed in Table 1-3, average about 0.1%. Therefore, the statistical uncertainties make a negligible contribution to the discrepancy. Given other sources of experimental error, including the uncertainty in the activities, the exact compositions and densities of the constituents of the Rando Phantom used in the experiment, and some observed anatomical differences between the experimental and voxel phantoms, we conclude that the MCNP model has been validated for these four nuclides.

The discrepancy between the MCNP simulation of ^{90}Sr/^{90}Y sources and the observed count rates is much greater than for the other nuclides. One reason is the complexity of the theoretical

---

[8] For the count rates of 6 kcps – 13 kcps, recorded in Table 1-3, the behavior of a paralyzable and a nonparalyzable system is essentially the same.

[9] The rms difference is calculated as $\Delta_{rms} = \sqrt{\frac{\sum_{i=1}^{n}\left(\frac{x_i}{y_i}-1\right)^2}{n}}$, where x_i and y_i are the individual corrected and calculated values, respectively, and n = 8.

model of β-bremsstrahlung production, compared to the models of γ-ray or x-ray interactions. In the latter case, given an accurate photon emission spectrum, the transport model utilizes the cross-sectional data used by the code, which is based on the ENSDF, to compute the scattering and absorption of the photons in the region between the source and the detector. Most of the interactions are due to the Compton effect and are therefore not strongly dependent on the exact composition of the surrounding media.

Table 2-4. Count Rates on Siemens e.cam Camera, Corrected for Dead-time Losses (cps/Bq)

Nuclide	MCNP		Experimental – corrected		Difference (%)		
	Anterior	Posterior	Anterior	Posterior	Anterior	Posterior	Average
Co-60	1.34e-01	1.45e-01	1.41e-01	1.35e-01	5.2	-7.1	-1.0
Sr-90/Y-90	2.65e-03	3.16e-03	4.24e-03	4.42e-03	60	40	50
Cs-137	8.85e-02	9.92e-02	9.55e-02	9.35e-02	7.9	-5.7	1.1
Ir-192	2.97e-01	3.41e-01	2.99e-01	3.08e-01	0.8	-9.4	-4.3
Am-241	3.37e-02	4.04e-02	3.96e-02	3.88e-02	17.4	-4.0	6.7

Note: Based on total count rates in all energy channels

On the other hand, the generation of photons following the β decay of ^{90}Sr and ^{90}Y is much more complicated. First, unlike the line spectra that characterize the photon emissions of the other four nuclides, β spectra have continuous energy distributions. As was mentioned earlier, we employed cubic spline interpolation to created a spectrum that had a higher resolution than the one furnished in the available data tables. However, the resulting energy distribution may not accurately represent the actual spectrum. Second, bremsstrahlung production is strongly dependent on the elemental composition of the medium in the vicinity of the source. Therefore, any deviation in the composition of the Rando Phantom from the values in our model, or any inhomogeneity in the material, would affect the bremsstrahlung. Finally, the bremsstrahlung production cross-sections for light elements have not been determined to the same level of accuracy as the photon scattering cross-sections.

In summary, the MCNP simulation of count rates from β bremsstrahlung is a two-step process, and is subject to the uncertainty of the bremsstrahlung production efficiency as well as to any uncertainties in the subsequent transport of the photons. The average discrepancy of 50% in the count rates from ^{90}Sr/^{90}Y recorded by the gamma camera should be understood in this context. Comparable discrepancies are found in the experimental measurements of this nuclide using the other three instruments, described in the following sections of this report.

2.2.2 Simulation of Thyroid Probe

The results of the MCNP analyses of the thyroid probe are listed in Table 2-5, together with the statistical uncertainties. The observed count rates, which were previously shown in Table 1-4, are listed as well. As seen in Table 2-5, the MCNP calculations for ^{60}Co and ^{192}Ir agree very well with the experimental results, the differences being comparable to the statistical uncertainties of the measurements and the calculations. The agreement with the ^{241}Am results is poorer. The

measured count rates from $^{90}Sr/^{90}Y$ are significantly higher than the calculated values, while the ^{137}Cs results exhibit a still greater discrepancy.

Table 2-5. Count Rates on Atomlab 950 Thyroid Uptake System

Nuclide	MCNP				Experiment				Difference (%)		
	Anterior		Posterior		Anterior		Posterior		Ant.	Post.	Ave.
	cps/Bq	C_v[a] (%)	cps/Bq	C_v (%)	cps/Bq	C_v (%)	cps/Bq	C_v (%)			
Co-60	4.64e-04	0.8	4.82e-04	0.8	4.69e-04	1.9	4.96e-04	1.8	1.0	2.9	1.9
Sr-90/Y-90	5.01e-06	5.1	6.59e-06	4.4	6.27e-06	2.3	7.82e-06	1.9	25	19	22
Cs-137	2.10e-04	0.9	2.26e-04	0.9	3.01e-04	1.6	3.24e-04	1.5	43	43	43
Ir-192	6.34e-04	0.9	7.16e-04	0.9	6.31e-04	1.4	7.12e-04	1.3	-0.6	-0.6	-0.6
Am-241	6.84e-05	1.3	8.44e-05	1.2	5.59e-05	1.8	7.30e-05	1.5	-18	-14	-16

[a] Coefficient of variation

The discrepancy in the $^{90}Sr/^{90}Y$ values is attributed to the same difficulties in simulating β-bremsstrahlung production that were discussed in the preceding section. The large discrepancy in the ^{137}Cs results is attributed to experimental error, most likely involving the position of the sources or the phantom. Nevertheless, the good agreement with the ^{60}Co and ^{192}Ir measurements, and the fair agreement for ^{241}Am, validate the model to an acceptable level of accuracy.

2.2.3 Simulation of Survey Meter

The results of the MCNP analyses of the survey meter are listed in Table 2-6, together with the count rates, derived from the observed exposure rates, which were shown earlier in Table 1-5. The statistical uncertainties in the MCNP calculations range from 0.36% for simulations of ^{137}Cs and ^{192}Ir with the meter in the posterior position to 1.7% for simulations of ^{90}Sr measured in the anterior position. These uncertainties are much smaller than the experimental uncertainties discussed in Section 1.3.3 and would therefore have little effect on the agreement between the calculations and the experiments.

Table 2-6. Count Rates on Ludlum Model 19A Micro R Meter (cps/Bq)

Nuclide	MCNP		Experiment		Difference (%)		
	Anterior	Posterior	Anterior	Posterior	Anterior	Posterior	Average
Co-60	1.95e-03	2.25e-03	1.8e-03	1.8e-03	-7.4	-20	-14
Sr-90/Y-90	2.24e-05	3.56e-05	3.5e-05	4.0e-05	55	13	34
Cs-137	1.07e-03	1.27e-03	9.4e-04	9.4e-04	-12	-26	-19
Ir-192	3.41e-03	5.06e-03	3.3e-03	4.3e-03	-2.2	-14	-8.3
Am-241	2.17e-04	3.67e-04	2.5e-04	2.9e-04	13	-22	-4.4

Additional uncertainty in the MCNP model stems from the positions of the sources with respect to the detector. Given the small physical size of the NaI(Tl) crystal and its close proximity to the

sources, any minor errors in the locations of the sources would have a much greater impact than in the experiments on the gamma camera and the thyroid probe. The data in Table 2-6 indicate a negative bias in the measurements in the posterior position: the differences between the matched pairs of values (MCNP – experiment) for the posterior position have consistently lower algebraic values than for the anterior. Since the same instrument was used in both cases, the differences are most likely due to anatomical differences between the physical phantom and the MCNP voxel model. These differences are also observed in the results for the gamma camera (which employed two separate detectors) and the waste monitor.

The rms difference for the eight sets of values for the four γ emitters is 16%, indicating a reasonable agreement, consistent with the inherent accuracy of the instrument and its potential use as a preliminary screening tool. The count rates derived from the measured exposure rates for ^{90}Sr/^{90}Y are again significantly higher than the calculated values.

2.2.4 Simulation of Waste Monitor

The results of the MCNP simulations of the waste monitor are shown in Table 2-7, together with the count rates, derived from the observed exposure rates, which were shown earlier in Table 1-6. The statistical uncertainties in the MCNP calculations range from 0.34% for simulations of ^{137}Cs measured from the posterior position to 1.7% for simulations of ^{90}Sr from the anterior position. These uncertainties are much smaller than the experimental uncertainties discussed in Section 1.3.4 and would therefore have little effect on the agreement between the calculations and the experiments. The results for all five nuclides are in reasonable agreement, given the experimental error and the aforesaid uncertainty in the bremsstrahlung yield.

Table 2-7. Count Rates on Ludlum Model 3530 Waste Monitor (cps/Bq)

Nuclide	MCNP		Measured		Difference (%)		
	Anterior	Posterior	Anterior	Posterior	Anterior	Posterior	Average
Co-60	2.67e-03	2.95e-03	3.0e-03	3.0e-03	11	0.9	6.2
Sr-90/Y-90	3.44e-05	4.55e-05	4.7e-05	5.5e-05	38	22	30
Cs-137	1.46e-03	1.66e-03	1.5e-03	1.5e-03	6.0	-6.7	-0.4
Ir-192	4.46e-03	5.62e-03	4.6e-03	4.6e-03	2.5	-19	-8
Am-241	4.44e-04	6.19e-04	3.4e-04	3.9e-04	-24	-36	-30

Chapter 3

DERIVATION OF CALIBRATION FACTORS

A final set of MCNP simulations was performed to predict the response of each of the four radiation detectors to activities in the lungs of an exposed individual. These analyses combined the model of each instrument, described in Chapter 2, with the NORMAN phantom, a high-resolution voxel model of the human body. The result of the analyses is a set of empirical relationships between the count rate or exposure rate of a given instrument and the lung burden of a given radionuclide. These relationships, expressed as normalized count rates or exposure rates, constitute a set of calibration factors for each of these instruments that permit them to be used to estimate these lung burdens.

3.1 NORMAN Phantom

The NORMAN (NORmal MAN) phantom was developed by the Health Protection Agency in the United Kingdom from an MRI scan of a volunteer (Jones 1997). The original data set comprised 35 million voxels; however, just over a quarter of these formed the human body. HPA slightly increased the dimensions of the original 2 mm voxels to produce a phantom that was 176 cm high and weighed 73 kg, the size and weight of Reference Man (ICRP 2002).

The NORMAN data were converted to the MCNP input format by the Los Alamos National Laboratory. Densities and elemental compositions were assigned to 37 regions of the phantom, based on data on the corresponding tissues and organs presented in ICRU Publication 46 (ICRU 1992).

The full phantom includes the entire body with appendages. However, due to limitations imposed by the MCNPX code and the Microsoft Windows operating system on the size of the voxel lattice, the phantom was truncated to reduce the lattice size. The NORMAN phantom used in the present study is thus a subset of the HPA data set, comprising over 15 million voxels. It corresponds to the upper part of the body and is approximately 85 cm high—a frontal section of the phantom is shown in Figure 3-1. The activity of each radionuclide is uniformly distributed in the lungs of the phantom. Because the activity is confined to the lungs, excluding the lower part of the body has no significant effect on the results of the simulation.

3.2 Simulation of Gamma Camera Response to Activity in NORMAN Phantom

Figure 3-2 shows a sagittal section of the NORMAN phantom and its position with respect to the two heads of the Siemens e.cam gamma camera, which corresponds to the position of a patient undergoing a lung scan. Unlike normal clinical practice, where the patient's chest is pressed against the collimator, a separation, typically 5 cm, would be maintained between the detector and the phantom, as discussed in Section 1.3.1.

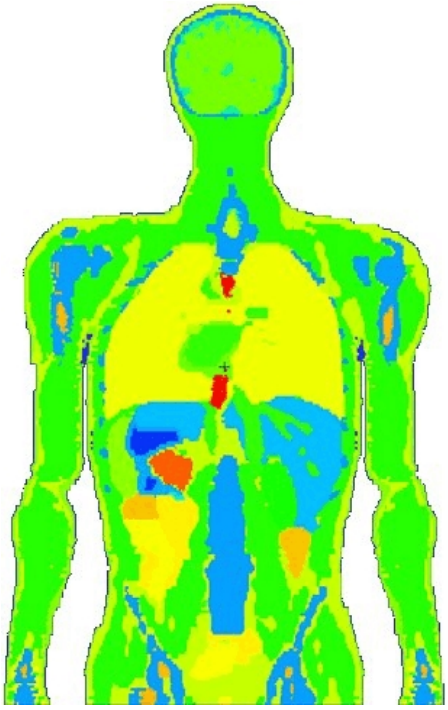

Figure 3-1. Frontal Section of NORMAN Phantom

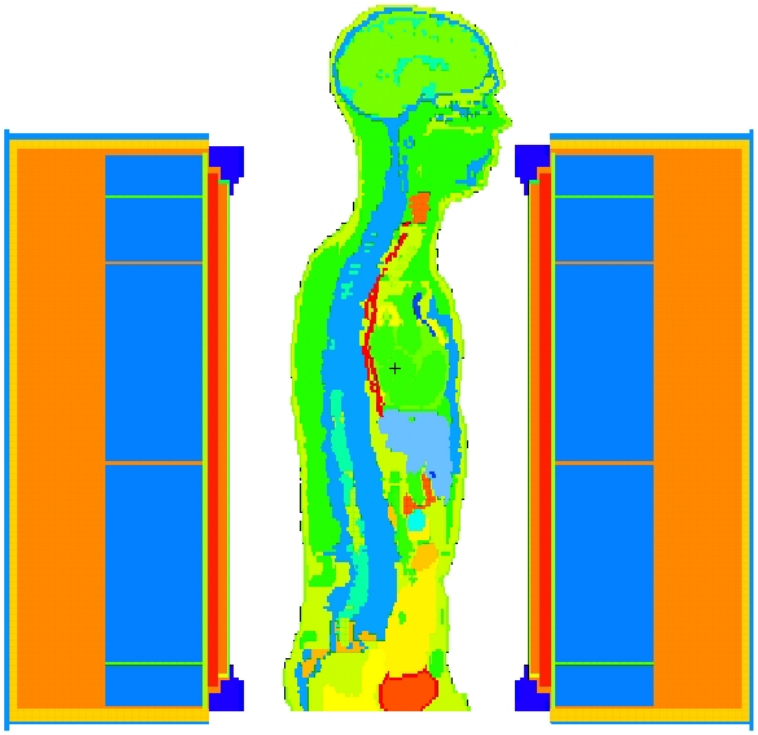

Figure 3-2. NORMAN Phantom and Siemens e.cam

3.2.1 Pulse Height Spectrum

In the MCNP simulations described in this chapter, the counts were tallied in 1-keV bins to enable the calculation of count rates over specific regions of the pulse height spectrum. Figure 3-3 shows the counts per source particle from ^{60}Co and ^{90}Sr/^{90}Y, as would be recorded by the detector in the anterior position. In order to permit the display of both spectra in a single graph, a different scale was used to plot the counts per energy interval from each nuclide.

These graphs are useful for understanding the energy distribution of the recorded pulses. Starting with ^{60}Co, we see that the spectrum has a strong Compton peak in the 50 – 250 keV region, which encompasses most of the counts registered on the camera. Note the small secondary peak at approximately 220 keV that is due to the superposition of backscattered Compton photons from the two ^{60}Co γ rays. These photons have a minimum energy of 210 keV, which corresponds to a 180º scatter of the 1,173 keV γ ray. This nuclide is thus readily detected by the Siemens e.cam, even though the main γ-ray energy peaks—1,332 and 1,173 keV—are beyond the energy range of the camera.

The pulse height spectrum from ^{90}Sr/^{90}Y bremsstrahlung x rays exhibits a peak at about 55 keV, with most of the counts falling in the range 20 – 150 keV. (Note that the uncertainty in the MCNP bremsstrahlung simulation may also affect the pulse height spectrum.)

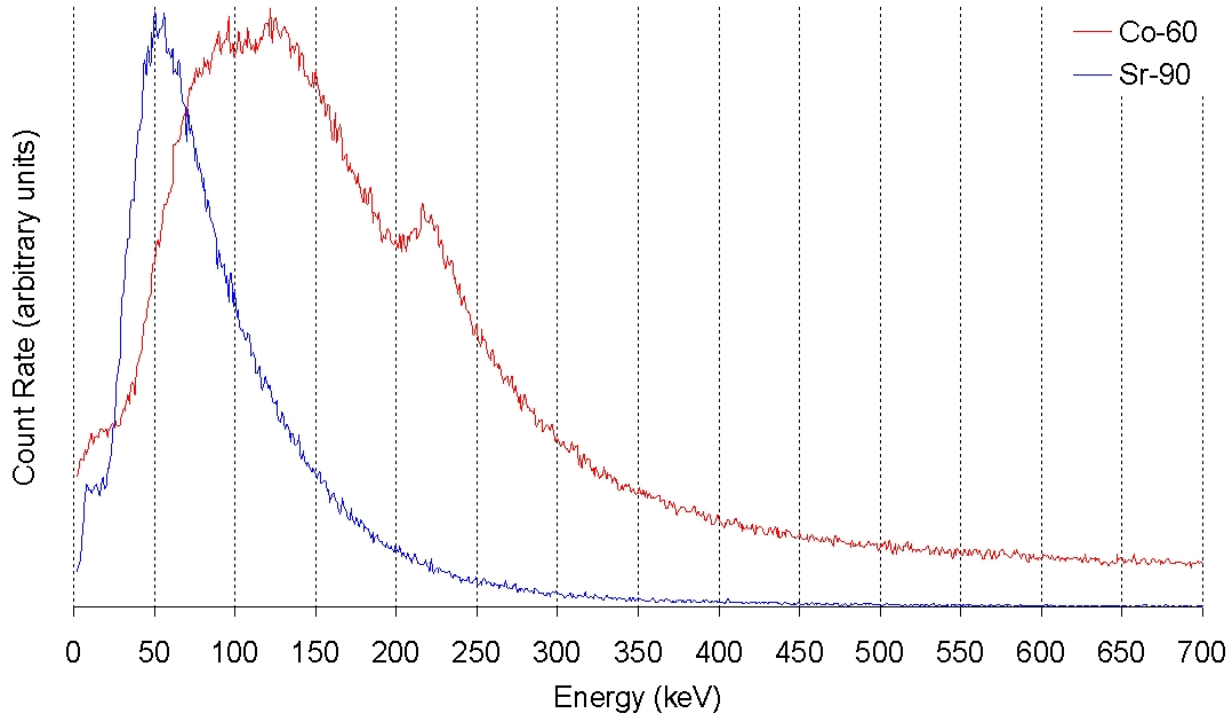

Figure 3-3. Count Rates on Siemens e.cam from Lung Burdens of ^{60}Co and ^{90}Sr

Figure 3-4 shows the corresponding pulse height spectra of ^{137}Cs, ^{192}Ir, and ^{241}Am. The photopeak of ^{137}Cs, at 662 keV, is just within the highest energy window that could be set on the camera used in the present study. However, as with ^{60}Co, most of the counts are from the Compton peak in the 50 – 250 keV region. There is again a Compton backscatter peak that has a minimum energy of 184 keV for this nuclide. Note also the prominent photopeak at 32 keV from cesium K x rays.

The ^{192}Ir spectrum includes a number of prominent photopeaks (listed in Table 2-2), as well as a broad Compton region. Most of the counts are within the 30 – 350 keV region.

The ^{241}Am spectrum primarily consists of pulses in the photopeak region. Almost all of the counts are within the range of 35 – 70 keV. Note the escape peak centered on 32 keV, the result of iodine K x rays escaping from the NaI(Tl) crystal.

3.2.2 Calibration Factors for Gamma Camera

The MCNP simulations were used to derive calibration factors for the gamma camera. Two sets of factors were developed. The first set, shown in Table 3-1, is based on the energy windows used in the experimental measurements that are listed in Table 1-2. Table 3-1 lists the normalized count rates in all three channels of the detectors in the anterior and posterior positions. The sum of the counts in the two detectors is also listed. The most reliable calibration factor is the total of the count rates from all channels in both detectors.

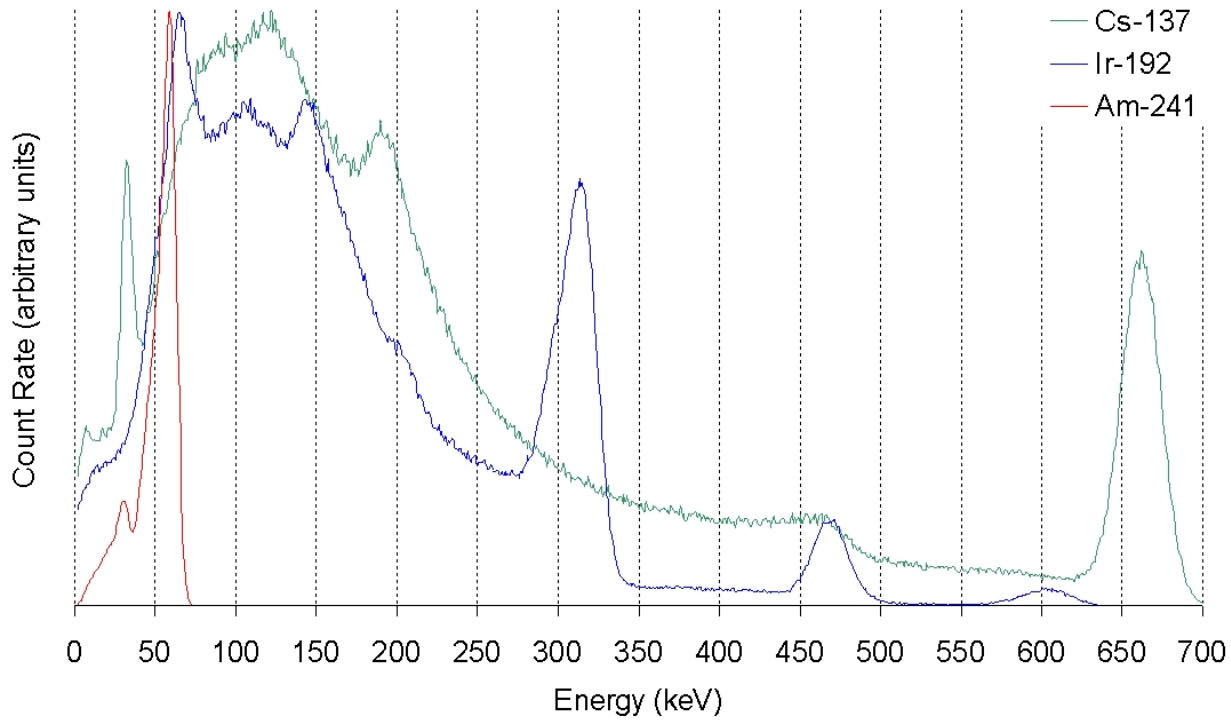

Figure 3-4. Count Rates on Siemens e.cam from Lung Burdens of ^{137}Cs, ^{192}Ir, and ^{241}Am

Because it may not always be practical to set six energy windows on the camera, we calculated new energy ranges for all the nuclides except ^{241}Am, based on three contiguous 50% energy windows. Each range was chosen to maximize the count rates from lung burdens of that nuclide, based on the spectra displayed in Figures 3-3 and 3-4. The calibration factors corresponding to these reduced energy ranges are shown in Table 3-2. No new factors were calculated for ^{241}Am, since the original calibration factors for this nuclide are based on only two energy windows.

Note that the total calibration factors (sums from all energy windows) for the four nuclides shown in Table 3-2 are 16% to 31% lower than the corresponding calibration factors in Table 3-1. As expected, the use of a narrower energy range leads to some loss of sensitivity.

3.3 Calibration Factors for Thyroid Probe

In the MCNP simulations of the thyroid probe, the anterior and posterior views were modeled with the detector 84.5 cm (~33 ¼ in) from the front and back of the NORMAN phantom, centered on the chest. At this distance, the entire lung region falls within the field of view of the conical collimator. This is greater than the distance of approximately 67 cm in the experimental measurements. The same energy range used in the experiments—20 to 1,499 keV—was used in these simulations. The calculated calibration factors are listed in Table 3-3.

Table 3-1. Calibration Factors for Siemens e.cam, Using Six 50% Energy Windows

Nuclide	Channel[a]	Normalized count rate (cps/Bq)		
		Anterior	Posterior	Total
Co-60	1	6.06e-03	6.08e-03	1.21e-02
	2	1.23e-01	1.27e-01	2.50e-01
	3	1.69e-02	1.71e-02	3.40e-02
	Total	1.46e-01	1.50e-01	2.96e-01
Sr-90/ Y-90	1	3.86e-04	3.21e-04	7.06e-04
	2	2.48e-03	2.38e-03	4.86e-03
	3	3.90e-05	3.78e-05	7.68e-05
	Total	2.90e-03	2.75e-03	5.64e-03
Cs-137	1	4.71e-03	4.38e-03	9.09e-03
	2	7.68e-02	7.83e-02	1.55e-01
	3	1.53e-02	1.49e-02	3.02e-02
	Total	9.68e-02	9.77e-02	1.95e-01
Ir-192	1	1.04e-02	1.02e-02	2.07e-02
	2	2.97e-01	2.97e-01	5.95e-01
	3	1.34e-02	1.32e-02	2.66e-02
	Total	3.20e-01	3.20e-01	6.41e-01
Am-241[b]	1	5.83e-03	5.21e-03	1.10e-02
	2	2.67e-02	2.34e-02	5.01e-02
	Total	3.24e-02	2.86e-02	6.10e-02

[a] See Table 1-2

[b] Only two windows were used for ^{241}Am, due to its narrow energy spectrum

3.4 Calibration Factors for Survey Meter

In the MCNP simulations of the survey meter, the anterior and posterior views were modeled with the housing 5 cm from the front and back, respectively, of the NORMAN phantom, with the sensitive element in the detector centered on the chest. In a clinical situation, holding the meter at this distance would be less intrusive than pressing it against the body of the exposed individual—it would also reduce the risk of contaminating the instrument. The calculated calibration factors are listed in Table 3-4. The factors are presented in terms of μR/h (the units displayed on the instrument) per Bq, based on a conversion factor of 175 cpm per μR/h.

3.5 Calibration Factors for Waste Monitor

As installed at Tisch Hospital, the waste monitor is not ideally positioned for assessing the lung burden of an exposed individual. Since the position of the monitor is fixed, the individual would have to kneel or sit in front of the monitor to align the detector with his chest. In the MCNP model, the anterior and posterior views were modeled with acrylic window shielding the detector

positioned 5 cm from the front and the back, respectively, of the NORMAN phantom, centered on the chest. The calculated calibration factors are listed in Table 3-5. The factors are presented in terms of μR/h (the units displayed on the instrument) per Bq, based on a conversion factor of 2,400 cpm per μR/h.

Table 3-2. Calibration Factors for Siemens e.cam, Using Three 50% Energy Windows

Nuclide	Peak (keV)	Normalized count rate (cps/Bq)		
		Anterior	Posterior	Total
Co-60	101.3	3.13e-02	3.26e-02	6.40e-02
	168.9	4.18e-02	4.32e-02	8.50e-02
	281.6	3.36e-02	3.39e-02	6.74e-02
	Total	1.07e-01	1.10e-01	2.16e-01
Sr-90/ Y-90	50.7	8.04e-04	7.46e-04	1.55e-03
	84.6	9.43e-04	9.14e-04	1.86e-03
	141.1	6.58e-04	6.45e-04	1.30e-03
	Total	2.41e-03	2.30e-03	4.71e-03
Cs-137	97.3	1.94e-02	2.01e-02	3.95e-02
	162.3	2.76e-02	2.80e-02	5.57e-02
	270.6	1.95e-02	1.96e-02	3.91e-02
	Total	6.65e-02	6.78e-02	1.34e-01
Ir-192	96	7.32e-02	7.54e-02	1.49e-01
	160.1	9.89e-02	9.89e-02	1.98e-01
	266.9	8.59e-02	8.46e-02	1.71e-01
	Total	2.58e-01	2.59e-01	5.17e-01

Note: See Table 3-1 for ^{241}Am calibration factors

Table 3-3. Calibration Factors for Atomlab 950 Thyroid Uptake System

Nuclide	Normalized count rate (cps/Bq)		
	Anterior	Posterior	Total
Co-60	4.16e-04	4.96e-04	9.12e-04
Sr-90/Y-90	5.00e-06	7.82e-06	1.28e-05
Cs-137	2.11e-04	3.24e-04	5.36e-04
Ir-192	6.18e-04	7.12e-04	1.33e-03
Am-241	5.85e-05	7.30e-05	1.32e-04

3.6 Minimum Detectable Activity (MDA)

The MARSSIM manual (NRC 2000) presents an analysis of the minimum activity that can be detected by a radiation measuring instrument. Based on that discussion, Anigstein et al. (2007,

Section 1.5) derived the following equation, which is used to calculate the minimum activities detectable by the instruments in the present study:

$$A_{ijk} = \frac{3 + 4.65\sqrt{b_{jk}\, t_c}}{n_{ijk}\, t_c} \qquad (3\text{-}1)$$

A_{ijk} = minimum activity of radionuclide *i* detectable by detector *j* in configuration *k* (Bq)[10]

n_{ijk} = normalized count rate of detector *j* in configuration *k* exposed to radionuclide *i* (cps/Bq)[11]

b_{jk} = background count rate of detector *j* in configuration *k* (cps)

t_c = counting time for both background and suspected radioactive source (S)

Table 3-4. Calibration Factors for Ludlum Model 19A Survey Meter

Nuclide	Normalized exposure rate (μR/h per Bq)		
	Anterior	Posterior	Total
Co-60	4.8e-04	4.8e-04	9.6e-04
Sr-90/Y-90	7.5e-06	6.8e-06	1.4e-05
Cs-137	2.7e-04	2.6e-04	5.4e-04
Ir-192	9.0e-04	8.6e-04	1.8e-03
Am-241	7.0e-05	6.0e-05	1.3e-04

Table 3-5. Calibration Factors for Ludlum Model 3530 Waste Monitor

Nuclide	Normalized exposure rate (μR/h per Bq)		
	Anterior	Posterior	Total
Co-60	2.4e-04	2.4e-04	4.8e-04
Sr-90/Y-90	3.4e-06	3.4e-06	6.7e-06
Cs-137	1.3e-04	1.3e-04	2.6e-04
Ir-192	4.1e-04	4.0e-04	8.1e-04
Am-241	3.9e-05	3.3e-05	7.2e-05

[10] "Configuration" refers to both the settings of the detector system (i.e., peak energy and width of energy window) and the source geometry (e.g., distance, position, and spatial distribution of activity in phantom).

[11] The normalized count rates comprise the calibration factors for the instruments in the present analysis.

In the following discussion, the minimum activities of the five radionuclides detectable by each of the four instruments are compared to the annual limits on intake (ALIs) via inhalation, based on the most restrictive chemical form (Eckerman et al. 1988). The purpose of the comparison is to present the reader with some qualitative basis of judging the suitability of these instruments for detecting lung burdens of these radionuclides. However, the numerical values of the ALIs are not strictly applicable to the assessment of inhaled activities, for reasons discussed below.

First, the ALI refers to the chronic intake via inhalation that will result in a committed dose of 5 rem (50 mSv) to an adult worker. However, only a fraction of such inhaled activity is retained in the body: the remainder (over 50% in the case of 1 μm AMAD particles) is promptly exhaled. Furthermore, only a fraction of the retained activity is localized in the region of the lungs. Immediately upon intake, approximately 15% of the total intake of 1 μm AMAD particles, or about 30% of the retained fraction, is deposited in the thoracic region, while the rest remains in the nasal and nasopharyngeal regions.[12] By the time radiation measurements are performed on the exposed individual, various fractions of the retained activity will have been either cleared from the body or redistributed among the various organs and tissues.

Second, the ALIs are based on the committed dose equivalents that are in turn based on the recommendations in ICRP Publication 26 (ICRP 1977). The more current dosimetric models, including those in Federal Guidance Report No. 13 (Eckerman et al. 1999), are based on the recommendations in ICRP Publication 60 (ICRP 1991). For the five radionuclides in the present study, the effective dose coefficients calculated by the more recent models are up to 3 times lower than the dose conversion factors that are the basis of the ALIs.

Nevertheless, comparing the MDAs to the ALIs provides a guide to the sensitivity of these instruments to lung burdens that could potentially affect the health of the exposed individual.

3.6.1 MDAs for Gamma Camera

Equation 3-1 was used to calculate the MDAs for the gamma camera, listed in Table 3-6. The results are tabulated for counting times of 1, 2, 5, and 10 minutes, assuming the same counting time is used for both the background and the assessment of the activity. The normalized count rates, n_{ijk}, were set equal to the total count rates from all three energy channels and both detectors that are listed in Table 3-1. The background counts were the total counts recorded in the two camera heads during the experimental measurements of each nuclide, as listed in Table 1-3. These MDAs are presented as examples of the detection efficiencies of this instrument. The actual MDA in a given application will depend on the background count rate on a given instrument at a given time. As shown in this table, the MDAs of all five nuclides are lower than the corresponding ALIs.

[12] These fractions are based on the respiratory tract model employed in Federal Guidance Report No. 13 (Eckerman et al. 1999).

Table 3-6. MDAs for Siemens e.cam, Using Six 50% Windows

Nuclide	ALI[a] (Bq)	Background[b] (cps)	Calibration factor[c] (cps/Bq)	Counting time (min)			
				1	2	5	10
				MDA (Bq)			
Co-60	1e+06	1,690	2.96E-01	84	59	37	26
Sr-90/Y-90	1e+05	1,679	5.64E-03	4,367	3,086	1,951	1,379
Cs-137	6e+06	1,690	1.95E-01	127	90	57	40
Ir-192	8e+06	1,679	6.41E-01	38	27	17	12
Am-241	200	298	6.10E-02	171	120	76	54

a Annual limits on intake for occupational exposure via inhalation, based on most restrictive chemical form (Eckerman et al. 1988)

b Total counts from both detectors recorded in experiment

c Total counts from both detectors (see Table 3-1)

3.6.2 MDAs for Thyroid Probe

The MDAs for the thyroid probe are listed in Table 3-7. The normalized count rates were set equal to the sums of the calibration factors for the anterior and posterior views, shown in Table 3-3. The background count rate used in the calculations is twice the average count rate recorded during the experimental measurements on the five nuclides, as listed in Table 1-4.[13] As shown in Table 3-7, the MDAs of ^{60}Co, ^{137}Cs, and ^{192}Ir are three to four orders of magnitude below the ALIs. To achieve an MDA of ^{90}Sr that is below the ALI would require a counting time of about 7.5 minutes.

Table 3-7. MDAs for Atomlab 950 Thyroid Uptake System

Nuclide	ALI (Bq)	Calibration factor[a] (cps/Bq)	Counting time (min)			
			1	2	5	10
			MDA (Bq)			
Co-60	1e+06	9.12e-04	3.19e+03	2.24e+03	1.41e+03	9.94e+02
Sr-90/Y-90	1e+05	1.28e-05	2.76e+05	1.94e+05	1.22e+05	8.61e+04
Cs-137	6e+06	5.36e-04	6.39e+03	4.49e+03	2.83e+03	1.99e+03
Ir-192	8e+06	1.33e-03	2.20e+03	1.55e+03	9.74e+02	6.87e+02
Am-241	200	1.32e-04	2.45e+04	1.73e+04	1.09e+04	7.66e+03
Background[b] (cps)		18.8				

a Total counts from anterior and posterior views (see Table 3-3)

b Twice the average background recorded in experiment (see text)

[13] The background counts were doubled to simulate the use of two virtual instruments—one in the anterior and one in the posterior position.

3.6.3 Detection Limits for Survey Meter and Waste Monitor

Since the survey meter and the waste monitor used in the measurements displayed zero background readings, it is not possible to use Equation 3-1 to calculate MDAs for these detectors. Instead, we calculated the minimum activities that would produce a significant scale reading on each of these instruments, which we define as 5 μR/h (the lowest marked division) on the survey meter and 1 μR/h on the waste monitor (see Figures 1-9 and 1-11 for illustrations of the meter scales of the two detectors). These activities, which are listed in Table 3-8, represent the practical lower detection limits of these instruments. As shown in this table, the detection limits of ^{60}Co, ^{137}Cs, and ^{192}Ir are well below the ALIs, while the limits on ^{90}Sr and ^{241}Am are up to two orders of magnitude higher than the respective ALIs.

Table 3-8. Detection Limits for Ludlum 19A Micro R Meter and Ludlum 3530 Waste Monitor

Nuclide	ALI[a] (Bq)	Detection limit (Bq)			
		19A Micro R Meter		3530 Waste Monitor	
		Anterior	Posterior	Anterior	Posterior
Co-60	1e+06	1.0e+04	1.0e+04	4.1e+03	4.2e+03
Sr-90/Y-90	1e+05	6.7e+05	7.4e+05	3.0e+05	3.0e+05
Cs-137	6e+06	1.8e+04	1.9e+04	7.6e+03	8.0e+03
Ir-192	8e+06	5.6e+03	5.8e+03	2.4e+03	2.5e+03
Am-241	200	7.1e+04	8.3e+04	2.6e+04	3.0e+04

3.7 Discussion

The calibration factors and MDAs of ^{90}Sr/^{90}Y are calculated on the assumption that the two nuclides are in secular equilibrium. This would not be the case if the ^{90}Sr had been produced or separated within a few days of the assessment. Such freshly produced material would result in a much lower count rate per unit activity in the lungs, leading to an underestimate of the actual activity. For aged material, the calibration factors for this decay chain could yield an overestimate of as much as 50%, based on comparisons of the calculated count rates with experimental measurements presented in Chapter 2. However, until a more accurate model of bremsstrahlung production from this decay chain is developed, we do not recommend reducing the calculated calibration factors. Use of the tabulated factors thus leads to a conservative assessment of this nuclide.

3.7.1 Siemens e.cam Gamma Camera

The calibration factors listed in Table 3-1, which are based on a mathematical model of the Siemens e.cam gamma camera that has been verified experimentally, would enable an assessment of the lung burden of one of the four γ emitters that is accurate to about 10%. We base this judgement on the comparison between the experimental measurements and the corresponding MCNP simulations, presented in Section 2.2.1. The calibration factors listed in Table 3-2 are somewhat less reliable because the response of the gamma camera over the

narrower energy ranges has not been experimentally verified. However, they are believed to give reasonable estimates of activities in the lungs. The accuracy of all the gamma camera calibration factors decreases at high count rates—corrections for dead-time counting losses should be applied for count rates well above 10 kcps per detector.

These calibration factors are strictly applicable only to an adult male of average height and weight, and only if his position with respect to the camera heads is the similar to that of the NORMAN phantom in Figure 3-2. Furthermore, these factors only apply to activities in the lungs. They are not accurate for the assessment of activity in the extrathoracic airways, nor of activity that has passed into the blood stream and been redistributed to other organs.

Finally, the calibration factors are derived specifically for the Siemens e.cam gamma camera. Other gamma camera systems, although employing similar NaI(Tl) detectors, will in general have different responses to these radiation sources due to differences in energy windows and other factors.

Future studies are planned that will expand the calibration factors to encompass juveniles of different ages and adults of both sexes. Biokinetic models will be used to calculate the distribution of radioactive materials in various tissues and organs as a function of time after intake. The planned calibration factors will combine the activities calculated by these models with the response of the gamma camera to activities in regions of the body other than the lungs. These factors will enable clinical personnel to estimate intakes based on the count rates at various times after time of exposure. Finally, calibration factors will be developed for other models of gamma cameras commonly used in the United States.

3.7.2 Atomlab 950 Thyroid Uptake System

The MCNP simulations of the response of the Atomlab 950 Thyroid Uptake System to sources in the Rando Phantom, discussed in Section 2.2.2, showed some discrepancies with the experimental measurements. Furthermore, the exposure geometry used in the derivation of the calibration factors, one which would encompass a full view of the lungs by the detector, was not experimentally verified. Consequently, assessments using these calibration factors could have uncertainties of 25% to 50%.

3.7.3 Ludlum Model 19A Survey Meter

The use of the Ludlum Model 19A survey meter for assessing lung burdens involves uncertainties in the positioning of the meter and in reading the meter scale, as discussed in Section 1.3.3. In addition, the observed discrepancies between the experimental measurements and the corresponding MCNP simulations discussed in Section 2.2.3 lead us to conclude that the calibration factors for this meter are accurate to about ± 25% for the three high-energy γ emitters: ^{60}Co, ^{137}Cs, and ^{192}Ir.

3.7.4 Ludlum Model 3530 Waste Monitor

The use of the Ludlum Model 3530 Waste Monitor for assessing lung burdens also involves uncertainties in reading the meter scale, especially for activities that produce low scale readings (< 5 μR/h). These uncertainties, as well as the comparison of the experimental measurements and the corresponding MCNP simulations presented in Section 2.2.4, lead us to conclude that the accuracy of the calibration factors for this instrument ranges from ± 20% to ± 50%, depending on the nuclide and its activity.

3.8 Conclusions

The gamma camera without a collimator is by far the most sensitive and accurate of the four instruments for detecting any of the five radionuclides in the lungs of an exposed individual. It is the only one of these instruments that can reliably assess lung burdens of ^{90}Sr or ^{241}Am that are below the ALIs. However, caution should be used in counting individuals with high internal activities, especially of energetic γ emitters such as ^{60}Co, ^{137}Cs, and ^{192}Ir. Lung burdens of these nuclides on the order of 1 MBq (~30 μCi) could result in pronounced dead-time counting losses which would lead to an underestimate of the lung burden. If such high activities are suspected, the exposed individual should first be screened with an appropriate hand-held instrument, such as a survey meter equipped with an ionization chamber.

The thyroid probe is less sensitive than the gamma camera, both because it has a smaller detector, and because the probe must be used at a distance from the exposed individual, due to the narrow field of view of the conical collimator. It is suitable for screening individuals for lung burdens of ^{60}Co, ^{137}Cs, or ^{192}Ir, but will produce a less accurate assessment than the gamma camera. This instrument could also experience count-rate losses if exposed to hundreds of MBq (several mCi) of these nuclides. It not sufficiently sensitive to be used for screening for lung burdens of ^{90}Sr or ^{241}Am.

Both the survey meter and the waste monitor are less sensitive than the other two instruments. They are useful in screening for lung burdens of the high-energy γ emitters—^{60}Co, ^{137}Cs, and ^{192}Ir—but are not suitable for screening for ^{90}Sr or ^{241}Am.

As discussed in Section 3.7.1, the calibration factors presented in this report apply only to activities in the lungs at the time of the measurement. They do not account for the clearance of radionuclides from the lungs following inhalation, nor for contributions to the count rates from radionuclides that have migrated to other organs or tissues (see discussion on page 31). The estimate of lung burdens based on the count rates in the detectors is not a sufficient basis for performing a radiological assessment of the exposed individual without accounting for these additional factors.

REFERENCES

Anigstein, R., et al. 2007. "Use of Radiation Detection, Measuring, and Imaging Instruments to Assess Internal Contamination from Intakes of Radionuclides. Part I: Feasibility Studies." http://www.bt.cdc.gov/radiation/clinicians/evaluation/pdf/Part_I.pdf

Baechler, S., et al. 2006. "Feasability of the Gamma Camera Acceptance Testing Procedure Introduced by the Swiss Federal Office of Public Health." www.colloquium.fr/06IRPA/CDROM/docs/P 054.pdf

Chu, S. Y. F., L. P. Ekström, and R. B. Firestone. 1999. "WWW Table of Radioactive Isotopes." http://nucleardata.nuclear.lu.se/nucleardata/toi/

Cristy, M., and K. F. Eckerman. 1987. "Specific Absorbed Fractions of Energy at Various Ages from Internal Photon Sources. I. Methods," ORNL/TM-8381/V1. Oak Ridge, TN: Oak Ridge National Laboratory.

The DOE/NRC Interagency Working Group on Radiological Dispersal Devices (DOE/NRC). 2003. "Radiological Dispersal Devices: An Initial Study to Identify Radioactive Materials of Greatest Concern and Approaches to Their Tracking, Tagging, and Disposition." www.ssa.doe.gov/sp70/documents/RDDRPTF14MAY03.pdf

Eckerman, K. F. (Oak Ridge National Laboratory). 2006. <eckermankf@ornl.gov> "Re: Histogram of beta spectra" June 2, 2006, personal e-mail to Robert Anigstein, SC&A, Inc.

Eckerman, K. F., et al. 1999. "Cancer Risk Coefficients for Environmental Exposure to Radionuclides," Federal Guidance Report No. 13, EPA-402/R-99-001. Oak Ridge, TN: Oak Ridge National Laboratory.

Eckerman, K. F., M. Cristy, and J. C. Ryman. 1996. "The ORNL Mathematical Phantom Series." http://homer.hsr.ornl.gov/VLab/mird2.pdf

Eckerman, K. F., A. B. Wolbarst, and A. C. B. Richardson. 1988. "Limiting Values of Radionuclide Intake and Air Concentration and Dose Conversion Factors for Inhalation, Submersion, and Ingestion," Federal Guidance Report No. 11, EPA-520/1-88-020. Washington, DC: U.S. Environmental Protection Agency, Office of Radiation Programs.

Hendricks, J. S., et al. 2006. "MCNPX, Version 26C," LA-UR-06-7991. http://mcnpx.lanl.gov/

International Commission on Radiological Protection (ICRP). 1977. "Recommendations of the ICRP," ICRP Publication 26. *Annals of the ICRP, 1*(3). Oxford: Pergamon Press.

International Commission on Radiological Protection (ICRP). 1991. "1990 Recommendations of the ICRP," ICRP Publication 60. *Annals of the ICRP, 21*(1-3). Oxford: Pergamon Press.

International Commission on Radiological Protection (ICRP). 2002. "Basic Anatomical and Physiological Data for Use in Radiation Protection: Reference Values," ICRP Publication 89. Annals of the ICRP, 32(3–4). Oxford: Pergamon Press.

International Commission on Radiation Units and Measurements (ICRU). 1992. "Photon, Electron, Proton and Neutron Interaction Data for Body Tissue," ICRU Report 46. Bethesda, MD: Author.

Jones, D. G. 1997. "A Realistic Anthropomorphic Phantom for Calculating Organ Doses Arising from External Photon Irradiation." *Radiation Protection Dosimetry, 72*(1), 21–29.

Los Alamos National Laboratory (LANL), X-5 Monte Carlo Team, Diagnostics Applications Group. 2004. "MCNP - A General Monte Carlo N-Particle Transport Code, Version 5." http://www-xdiv.lanl.gov/x5/MCNP/pdf/MCNP5_manual_VOL_I.pdf

Los Alamos National Laboratory (LANL). 2006. "MCNPX." http://mcnpx.lanl.gov/

Ludlum Measurements, Inc. 2000. "Ludlum Model 19A Micro R Meter." Sweetwater, TX: Author. http://www.ludlums.com/manuals/M19Aoct00.pdf

Nuclear Regulatory Commission (U.S.) (NRC). 2000. "Multi-Agency Radiation Survey and Site Investigation Manual (MARSSIM)," NUREG-1575, Rev. 1. Washington, DC: Author.

"The Phantom Laboratory." n/d. http://www.phantomlab.com/rando.html

Shrimpton, P. C., B. F. Wall, and E. S. Fisher. 1981. "The Tissue-Equivalence of the Alderson Rando Anthropomorphic Phantom for X-rays of Diagnostic Qualities." *Physics in Medicine and Biology, 26,* 133–139.

Siemens Medical Solutions USA, Inc. 2005. "e.cam Fixed 180." http://cardiology.usa.siemens.com/products-and-it-systems/cardiology-products/nuclear-cardiology/e-cam-fixed-180/e-cam-fixed-180.aspx

Tokai Research Establishment, JAERI. 2001. DECDC 1.0: Nuclear Decay Data Files for Radiation Dosimetry Calculations, DLC-213, RSICC Data Library Collection [Computer software and manual]. Oak Ridge, TN: Oak Ridge National Laboratory.

Wang, B., X. G. Xu, and C. H. Kim. 2004. "A Monte Carlo CT Model of the Rando Phantom." *American Nuclear Society Transactions*, *90*, 473-474.

White, D. R. 1978. "Tissue Substitutes in Experimental Radiation Physics." *Medical Physics, 5*(6), 467–479.